IEEE Access
Multidisciplinary : Rapid Review : Open Access Journal

Received August 20, 2020, accepted October 13, 2020, date of publication October 15, 2020, date of current version October 28, 2020.

Digital Object Identifier 10.1109/ACCESS.2020.3031369

Recent Advances in High Frequency Modeling by Means of Domain Confinement and Nested Kriging

SLAWOMIR KOZIEL[1,2], (Senior Member, IEEE), AND ANNA PIETRENKO-DABROWSKA[2], (Senior Member, IEEE)

[1]Engineering Optimization and Modeling Center, Department of Engineering, Reykjavik University, 101 Reykjavik, Iceland
[2]Faculty of Electronics, Telecommunications, and Informatics, Gdansk University of Technology, 80-233 Gdansk, Poland

Corresponding author: Anna Pietrenko-Dabrowska (anna.dabrowska@pg.edu.pl)

This work was supported in part by the Icelandic Centre for Research (RANNIS) under Grant 206606051, and in part by the National Science Centre of Poland under Grant 2017/27/B/ST7/00563.

ABSTRACT Development of modern high-frequency components and circuits is heavily based on full-wave electromagnetic (EM) simulation tools. Some phenomena, although important from the point of view of the system performance, e.g., EM cross-coupling effects, feed radiation in antenna arrays, substrate anisotropy, cannot be adequately accounted for using simpler means such as equivalent network representations. Consequently, the involvement of EM analysis, especially for tuning of geometry parameters, has become imperative in high-frequency electronics. Notwithstanding, excessive computational costs associated with massive full-wave simulations required by these procedures and even more by tasks such as uncertainty quantification or multi-criterial optimization, constitute a practical bottleneck. Repetitive evaluations of a structure can be facilitated by the use of fast replacement models (surrogates). Among available methods, approximation models are by far the most popular due to their flexibility and accessibility. Unfortunately, surrogate modeling of high-frequency structures is hindered by the curse of dimensionality and nonlinearity of system responses, primarily frequency characteristics. The recently proposed performance-driven techniques attempt to address this issue by appropriate confinement of the model domain to focus the modeling process only on the relevant part of the parameter space, i.e., containing the designs that are of high quality from the point of view the assumed performance figures. The nested kriging framework is perhaps the most advanced of these methods and allows for constructing reliable surrogates over broad ranges of the system parameters and operating conditions. This article summarizes the recent developments of the technique, including the basic formulation and several advancements aiming at the improvement of the surrogate predictive power or lowering the computational cost of training data acquisition. These include the incorporation of sensitivity data, as well as dimensionality reduction through principal component analysis. The problem of uniform data sampling in confined domains is also discussed. Our considerations are comprehensively illustrated using several examples of antennas and microwave circuits.

INDEX TERMS High-frequency design, electromagnetic simulation, surrogate modeling, performance-driven modeling, domain confinement, nested kriging, design optimization.

I. INTRODUCTION

High-frequency electronics has been rapidly expanding over the recent years. A number of new application areas have been emerging, such as remote sensing [1], internet of things (IoT) [2], medical imaging [3], 5G technology [4], wearable and implantable devices [5], [6], to name just a few. These, but also more traditional areas, need components and devices (antennas, filters, couplers, etc.) of improved performance parameters [7], [8], multi-functionality [9], [10], and smaller physical sizes [11], [12]. The keystone of practical high-frequency design is undoubtedly full-wave electromagnetic (EM) analysis, which is the only tool capable of providing reliable evaluation of electrical and field properties of circuits

The associate editor coordinating the review of this manuscript and approving it for publication was Luca Cassano.

This work is licensed under a Creative Commons Attribution 4.0 License. For more information, see https://creativecommons.org/licenses/by/4.0/

of growing complexity. Accounting for the effects such as EM cross-couplings [13], [14], the presence of environmental components (connectors [15], housing [16]), or mutual coupling of radiators [17], is no longer possible using simplified representations, primarily analytical or equivalent network models. For many components and circuits of unconventional topologies, the employment of EM simulation is mandatory not just for design evaluation but in the design process itself, e.g., to verify the relevance of particular geometry amendments [18], and—even more importantly—to carry out the parameter tuning [19], [20], or to estimate the effects of manufacturing tolerances [21] and other types of uncertainties [22]. EM-driven design procedures may generate considerable computational expenses, often prohibitive. This is the reason for the continuous popularity of interactive design approaches, e.g., supervised parameter sweeping.

Accelerating simulation-based design procedures has been the subject of an extensive research and a number of methods have been developed to address different scenarios (single- [23] and multi-objective optimization [24], uncertainty quantification [25], robust design [26], global search [27]). Available solutions include expediting gradient-based algorithms by means of adjoint sensitivities [28], or sparse Jacobian updates [29]–[31], variable-fidelity techniques (space mapping [32], [33], response correction methods [34], [35]), exploitation of specific structure of the system response (feature-based optimization [36], [37], cognition-driven design [38]), as well as machine learning approaches [39], [40]. A reasonably large part of the aforementioned methods involves physics-based surrogates, where the problem-specific knowledge embedded in the lower-fidelity model (e.g., equivalent network [41]) can be employed to construct a reliable prediction tool facilitating identification of the improved designs at a low cost [42]. The low-fidelity model correction is typically arranged using the high-fidelity EM data accumulated along the optimization path [43]. In the case of global optimization, the surrogates are often of data-driven type [44] and constructed iteratively using sequential sampling techniques [45].

An overall replacement of expensive EM simulations by metamodels is a conceptually attractive alternative to the methods outlined in the previous paragraph. Availability of fast surrogate enables execution of all kinds of simulation-based design procedures at nearly negligible costs. Data-driven modeling methods are among the most popular ones due to their versatility, low-evaluation cost, and easy access through various toolboxes implemented in popular programming environments, mostly Matlab (e.g., [46], [47]). Widely used techniques include polynomial regression [48], radial basis functions [49], kriging [50], support vector regression [51], artificial neural networks [52], as well as polynomial chaos expansion [53]. Unfortunately, approximation-modeling methods are severely affected by the curse of dimensionality, i.e., a rapid increase in the number of training data samples necessary to render a surrogate of the assumed accuracy. Furthermore, in order for the model to exhibit practical design utility, its region of validity should cover sufficiently broad ranges of the system parameters and operating conditions [54]. This, along with typically high nonlinearity of the system responses, makes the modeling process even more challenging. Realistically, conventional data-driven models are capable of handling structures described by a few parameters [55], [56]. Physics-based surrogates are more immune to these issues but their applicability is subject to the existence and the quality of the underlying low-fidelity model [57].

There are several methods that can be used to address the aforementioned problems to a certain extent. High-dimensional model representation (HDMR) [58] represents the system output using an expansion of a multivariable function in the form of a sum of components being functions of individual variables, pairs of variables, etc. This allows for taking into account the most important relationships between the parameters and potentially reduce the cost of training data acquisition. The methods such as variable screening [59], global sensitivity analysis (e.g., Sobol indices [60]), or principal component analysis (PCA) [61] can be used for detecting variable correlations and reduce the parameter space dimensionality by restricting the modeling process only to the most significant directions or parameter subsets. A different approach is taken by orthogonal matching pursuit (OMP) [62] or least-angle regression [63], which focus on selecting the suitable basis functions for the surrogate models and, in particular, allow for solving underdetermined regression problems. Finally, variable-fidelity methods attempt to reduce the computational cost of model construction by combining densely sampled low-fidelity data with sparsely allocated high-fidelity data (e.g., co-kriging [64], Bayesian model fusion [65], two-stage Gaussian process regression [66]), which works well if sufficiently accurate low-fidelity models (i.e., well correlated with the high-fidelity one) are available.

Performance-driven surrogates [67]–[70], constitute an alternative way of alleviating the difficulties of conventional approximation modeling. The basic idea is to restrict the model domain to a region containing high quality designs with respect to the considered performance figures. The latter may include operating frequencies, bandwidths, but also material parameters (e.g., permittivity of the substrate the component is to be implemented on). The estimation of the region of interest is obtained using a set of pre-optimized reference designs [67] that can be known beforehand (e.g., from the prior design work with the same structure) or acquired specifically for the purpose of constructing the surrogate. The initial realizations of this concept only allowed to handle a single performance figure [67] or up to two figures with the structured allocation of the reference designs [68]. Further developments, e.g., triangulation-based modeling [69] enabled handling of arbitrary number of figures of interest but certain practical aspects such as design of experiments or model optimization were far from trivial.

The recent development of performance-driven modeling techniques is the nested kriging framework [70], where the

surrogate model domain is established using the auxiliary inverse model (so-called first-level surrogate), whereas the final model is constructed within that domain using kriging interpolation. The formulation of the nested kriging contains the mechanisms for uniform training data sampling and straightforward optimization of the surrogate, including generation of a reasonable starting point (for a given target vector of design objectives). The technique has been demonstrated to outperform conventional methods and to be capable of rendering reliable surrogates of antenna and microwave components over broad ranges of geometry and material parameters as well as operating conditions [70], [71]. Recently, further developments of the nested kriging technique have been reported that aim at the improvement of the model predictive power, reducing the computational cost of training data acquisition, as well as combining it with other methods. These include improved design of experiments strategy [72], automated adjustment of the lateral dimensions of the model domain [73], sensitivity-based first-level model [74], [75], combining nested kriging with response feature technology [76], or principal component analysis for dimensionality reduction of the model domain [77], [78]. The purpose of this article is to summarize the aforementioned recent advancements but also to provide a generic introduction to the nested kriging approach. Our considerations are illustrated using representative examples of antenna and microwave components.

II. NESTED KRIGING: BASIC FORMULATION

This section outlines a concept and provides a rigorous formulation of the basic version of the nested kriging framework [70]. In particular, we discuss the definition of the surrogate model domain, the first- and second-level models, as well as the sampling scheme. Demonstration example (a ring slot antenna) is also provided along with the results of benchmarking against conventional modeling methods.

A. NOTATION AND BASIC CONCEPTS

The rationale behind the nested kriging framework is that optimizing a given structure for the various sets of performance specifications (e.g., different operating frequencies) requires a synchronized adjustment of the system parameters [70]. Consequently, only those regions of the parameter space that adhere to these correlation patterns are of interest as containing high quality designs. From this perspective, constructing the surrogate model in a traditional, box-constrained domain, is a waste of computational resources. The first issue is an identification of such promising regions, which is realized by means of a set of so-called reference designs and the first-level surrogate model as described below.

We use the following notation. By $\boldsymbol{x} = [x_1 \ldots x_n]^T$ we denote the vector of the designable parameters. The conventional parameter space is denoted as X and defined as an interval $[\boldsymbol{l}, \boldsymbol{u}]$, where $\boldsymbol{l} = [l_1 \ldots, l_n]^T$ and $\boldsymbol{u} = [u_1 \ldots, u_n]^T$, are the lower and upper bounds on parameters; thus, we have $l_k \leq x_k \leq u_k$ for $k = 1, \ldots, n$. Furthermore, f_k, $k = 1, \ldots, N$, will stand for the figures of interest (e.g., operating frequency, bandwidth, or substrate permittivity). The objective space F is defined by the ranges $f_{k.\min} \leq f_{k(j)} \leq f_{k.\max}$, $k = 1, \ldots, N$. From the perspective of performance figures, F is the region of interest for surrogate model construction.

The surrogate model is to be rendered in the context of the objective space F. In particular, one needs to determine the meaning of high-quality designs, i.e., the designs that are optimal for given objective vectors $\boldsymbol{f} \in F$. This is understood in the sense of minimizing $U(\boldsymbol{x}, \boldsymbol{f})$, where U is the scalar merit function. More specifically, the optimum design $\boldsymbol{x}^*$ is given as

$$\boldsymbol{x}^* = U_F(\boldsymbol{f}) = \arg\min_{\boldsymbol{x}} U(\boldsymbol{x}, \boldsymbol{f}) \tag{1}$$

Furthermore, we define a manifold of designs that are optimum w.r.t. all $\boldsymbol{f} \in F$ as

$$U_F(F) = \{U_F(\boldsymbol{f}) : \boldsymbol{f} \in F\} \tag{2}$$

The nested kriging framework attempts to set up the surrogate in a possibly small region that contains $U_F(F)$. Construction of the said region involves the reference designs $\boldsymbol{x}^{(j)} = [x_1^{(j)} \ldots x_n^{(j)}]^T j = 1, \ldots, p$, obtained as $U_F(\boldsymbol{f}^{(j)})$ for the selected vectors $\boldsymbol{f}^{(j)} = [f_1^{(j)} \ldots f_N^{(j)}] \in F$ [70]. The data set $\{\boldsymbol{f}^{(j)}, \boldsymbol{x}^{(j)}\}$, $j = 1, \ldots, p$, is employed to construct the so-called first-level surrogate $\boldsymbol{s}_I(\boldsymbol{f})$: $F \rightarrow X$ [70]. The image $\boldsymbol{s}_I(F)$ of F is the first approximation of $U_F(F)$, see Fig. 1 for a graphical illustration. It should be emphasized that $\boldsymbol{s}_I(F)$ does not coincide with $U_F(F)$, therefore further operations are required to define the model domain as elaborated below; specifically, $\boldsymbol{s}_I(F)$ has to be somewhat extended in the lateral directions in order to encompass $U_F(F)$.

B. SURROGATE MODEL DOMAIN. DESIGN OF EXPERIMENTS

The aforementioned extension of $\boldsymbol{s}_I(F)$ is realized using the vectors normal to $\boldsymbol{s}_I(F)$ at $\boldsymbol{f}$, $\{\boldsymbol{v}_{n(k)}(\boldsymbol{f})\}$, $k = 1, \ldots, n - N$ [70]. Using the notation $\boldsymbol{x}_{\max} = \max\{\boldsymbol{x}^{(k)}, k = 1, \ldots, p\}$, $\boldsymbol{x}_{\min} = \min\{\boldsymbol{x}^{(k)}, k = 1, \ldots, p\}$, we define the vector $\boldsymbol{x}_d = \boldsymbol{x}_{\max} - \boldsymbol{x}_{\min}$ quantifying the parameter variations in $\boldsymbol{s}_I(F)$, as well as the extension coefficients

$$\begin{aligned}\boldsymbol{\alpha}(\boldsymbol{f}) &= [\alpha_1(\boldsymbol{f}) \ \ldots \ \alpha_{n-N}(\boldsymbol{f})]^T \\ &= 0.5T\left[|\boldsymbol{x}_d \boldsymbol{v}_n^{(1)}(\boldsymbol{f})| \ \ \ldots \ \ |\boldsymbol{x}_d \boldsymbol{v}_n^{(n-N)}(\boldsymbol{f})|\right]^T\end{aligned} \tag{3}$$

with T being a user-defined thickness parameter. The surrogate model domain X_S is then defined as

$$X_S = \left\{ \begin{array}{c} \boldsymbol{x} = \boldsymbol{s}_I(\boldsymbol{f}) + \sum_{k=1}^{n-N} \lambda_k \alpha_k(\boldsymbol{f}) \boldsymbol{v}_n^{(k)}(\boldsymbol{f}) : \boldsymbol{f} \in F, \\ -1 \leq \lambda_k \leq 1, \ k = 1, \ldots, n-N \end{array} \right\} \tag{4}$$

where

$$M_{\pm} = \left\{ \boldsymbol{x} \in X : \boldsymbol{x} = \boldsymbol{s}_I(\boldsymbol{f}) \pm \sum\nolimits_{k=1}^{n-N} \alpha_k(\boldsymbol{f}) \boldsymbol{v}_n^{(k)}(\boldsymbol{f}) \right\} \tag{5}$$

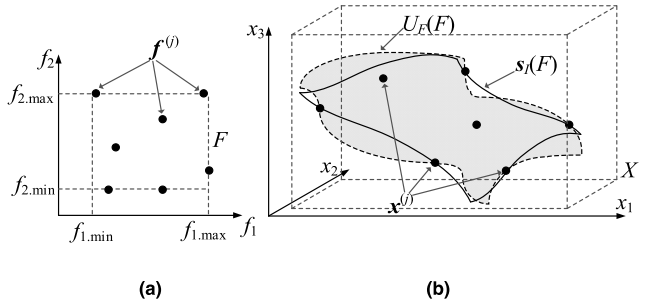

FIGURE 1. Basic concepts of the nested kriging framework (here, illustrated for two performance figures and a three-dimensional parameter space): (a) objective space F, (b) conventional parameter space X, the reference designs $x^{(j)}$, the optimum design manifold $U_F(F)$, and the first-level model image $s_I(F)$. The sets $U_F(F)$ and $s_I(F)$ are not identical: they coincide for all reference designs but not for all $f \in F$. Therefore, $s_I(F)$ has to be extended to encapsulate $U_F(F)$.

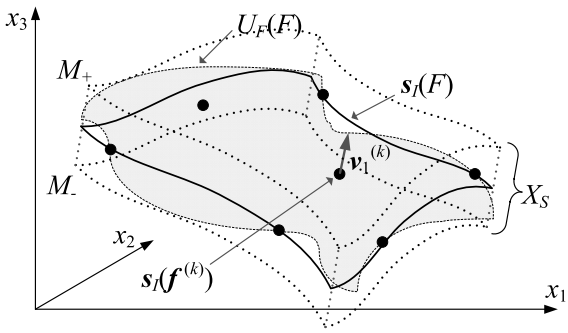

FIGURE 2. Surrogate model definition according to the nested kriging framework [70]. The picture shows the set $s_I(F)$, the normal vector $v_1^{(k)}$ at a selected objective vector $f^{(k)}$, the manifolds M_- and M_+ and the domain X_S obtained through orthogonal extension of $s_I(F)$.

Figure 2 provides a graphical illustration of the manifolds M_+, M_-, and the domain X_S. The final (second-level) surrogate is constructed in X_S using kriging interpolation [79] and the training data $\{\boldsymbol{x}_{B^{(k)}}, \boldsymbol{R}(\boldsymbol{x}_{B^{(k)}})\}_{k=1,\ldots,NB}$. Therein, $\boldsymbol{x}_{B^{(k)}} \in X_S$ are uniformly allocated samples, whereas $\boldsymbol{R}$ stands for the response of the EM-simulation model of the component/system at hand.

Domain confinement is computationally beneficial because X_S is dramatically smaller than the conventional domain X. As demonstrated in [70], it allows for constructing reliable surrogates without formally restricting the ranges of the system parameters and operating conditions of the structure.

Nested kriging provides convenient mechanisms for uniform data sampling and surrogate model optimization. Both are facilitated using a one-to-one mapping between the unit interval $[0, 1]^n$ and X_S. For the point $z \in [0, 1]^n$, the mapping h_1 [70]

$$\begin{aligned}\boldsymbol{y} = h_1(\boldsymbol{z}) = h_1([z_1 \ \ldots \ z_n]^T) = [f_{1.\min} + z_1(f_{1.\max} - f_{1.\min}) \\ \ldots \ldots f_{N.\min} + z_N(f_{N.\max} - f_{N.\min})] \\ \times [-1 + 2z_{N+1} \ \ldots \ -1 + 2z_n]\end{aligned} \tag{6}$$

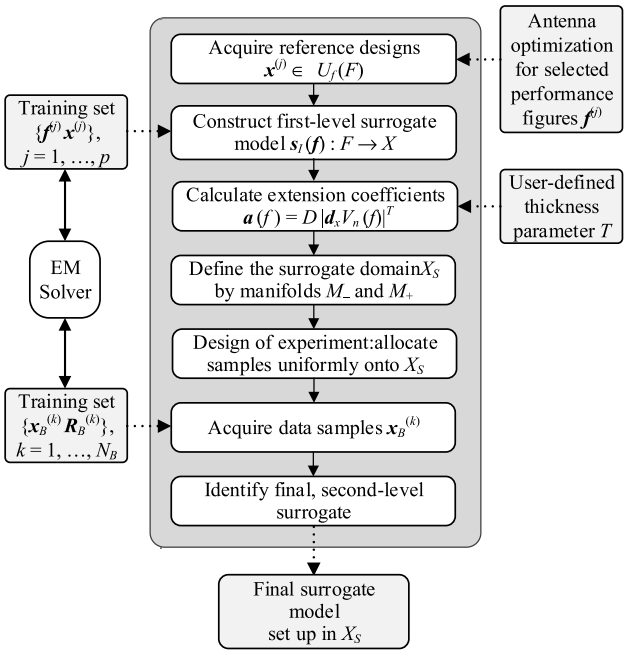

FIGURE 3. Flow diagram of the nested kriging framework [70].

transforms $[0, 1]^n$ onto the Cartesian product $F \times [-1, 1]^{n-N}$. In the next step, the function h_2 defined as

$$\begin{aligned}\boldsymbol{x} = h_2(\boldsymbol{y}) = h_2([y_1 \ \ldots \ y_n]^T) = \boldsymbol{s}_I([y_1 \ \ldots \ y_N]^T) \\ + \sum_{k=1}^{n-N} y_{N+k}\alpha_k([y_1 \ \ldots \ y_N]^T)\boldsymbol{v}_n^{(k)}([y_1 \ \ldots \ y_N]^T)\end{aligned} \tag{7}$$

maps $F \times [-1, 1]^{n-N}$ onto X_S. Finally, the data points $\boldsymbol{x}_{B^{(k)}}$ in X_S are generated as

$$\boldsymbol{x}_B^{(k)} = H(\boldsymbol{z}^{(k)}) = h_2(h_1(\boldsymbol{z}^{(k)})) \tag{8}$$

Here, $\{\boldsymbol{z}^{(k)}\}$, $k = 1, \ldots, N_B$, are uniformly distributed data points in $[0, 1]^n$, obtained using, e.g., Latin Hypercube Sampling [80].

The mapping H can also be used for model optimization, by reformulating the problem (1) defined on X_S into the following task

$$\boldsymbol{x}^* = \arg \min_{\boldsymbol{z} \in [0,1]^n} U(H(\boldsymbol{z}), \boldsymbol{f}) \tag{9}$$

which is solved in the normalized domain $[0, 1]^n$. Furthermore, a good initial design can be obtained as $\boldsymbol{x}^{(0)} = \boldsymbol{s}_I(\boldsymbol{f})$, which is the best approximation of $U_F(\boldsymbol{f})$ that one can get from the first-level surrogate.

C. NESTED KRIGING MODELING FRAMEWORK

The entire modeling process has been graphically represented in Fig. 3. The basic steps include acquisition of the reference designs, definition of the model domain, design of experiments and gathering the training data through EM simulation, as well as construction of the final surrogate.

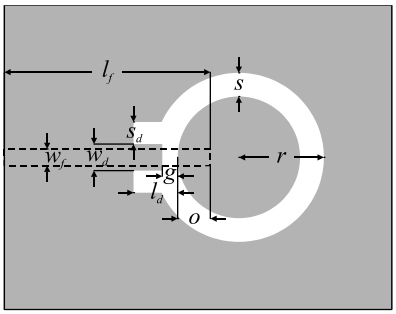

FIGURE 4. Ring slot antenna geometry. Feed line marked using a dashed line [81].

TABLE 1. Nested kriging: Modeling results for antenna of Fig. 4.

Number of training samples	Relative RMS Error				
	Conventional Models		Nested Kriging Model		
	Kriging	RBF	$D = 0.05$	$D = 0.1$	$D = 0.15$
50	56.9 %	61.0 %	12.9 %	19.4 %	25.1 %
100	50.8 %	53.2 %	6.9 %	12.9 %	16.5 %
200	35.8 %	37.9 %	4.9 %	7.7 %	12.7 %
400	31.5 %	34.1 %	3.1 %	5.1 %	9.0 %
800	25.6 %	27.2 %	2.2 %	3.7 %	6.2 %

D. NESTED KRIGING FOR ANTENNA MODELING

Operation and performance of the nested kriging framework is illustrated using the ring slot antenna example considered in [70], see Fig. 4. The structure is implemented on 0.76-mm-thick substrate and described by eight parameters $\boldsymbol{x} = [l_f\ l_d\ w_d\ r\ s\ s_d\ o\ g]^T$; ε_r is an additional variable (substrate permittivity) [81]. For any given ε_r, the feed line width w_f is calculated to ensure 50 ohm input impedance. The EM model is implemented in CST (∼300,000 cells, simulation 90 s).

The modeling goal was to render the surrogate valid for the antenna operating frequencies f within the range 2.5 GHz $\leq f \leq$ 6.5 GHz, and substrate permittivity ε_r within the range of $2.0 \leq \varepsilon_r \leq 5.0$. There are ten reference designs selected (cf. [70]). Table 1 shows the average relative RMS error for the nested kriging model constructed using three different values of the thickness parameter T and training data set sizes from 50 to 800 samples. In all cases, the nested kriging surrogate is more accurate than conventional models.

The dependence of the modeling error on T indicates that careful choice of this parameter is recommended, which is one of the practical issues of the technique (cf. Section III.B). Figure 5 shows the antenna responses for selected test designs, whereas Fig. 6 illustrates the results of model optimization for the selected target objective vectors. These experiments were carried out to demonstrate the design utility of the surrogate.

III. NESTED KRIGING: RECENT DEVELOPMENTS

Having presented the basic formulation and performance of the nested kriging framework, this section outlines the recent developments of the technique [72]–[77], [82], [83]. These were supposed to address particular aspects of the nested kriging, including further improvement of its predictive power [77], introduction of more efficient data sampling schemes [72], model setup automation [73], reduction of the computational cost of the model setup [74], [75] as well as incorporation of other algorithmic components, especially variable-fidelity simulations [82], [83] and response feature technology [76]. Sections III.A through III.F contain a brief exposition of these developments illustrated using examples of antenna and microwave components.

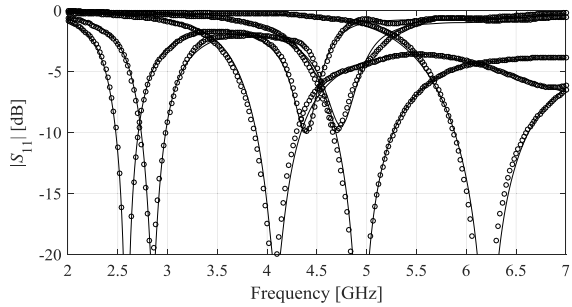

FIGURE 5. Ring slot antenna: reflection characteristics at the selected test designs for the surrogate constructed using nested kriging with N = 400 training samples and thickness parameter T = 0.05: EM model (—), surrogate (o).

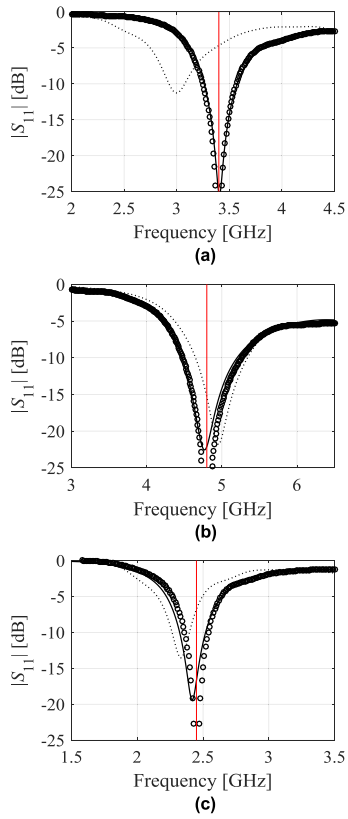

FIGURE 6. Ring slot antenna: nested surrogate (o) and EM-simulated responses (—) at the designs obtained by optimizing the surrogate model with $D = 0.1$ for (a) $f_1 = 2.45$ GHz, $f_2 = 5.3$ GHz, (b) $f_1 = 2.2$ GHz, $f_2 = 4.5$ GHz, and (c) $f_1 = 2.0$ GHz, $f_2 = 4.2$ GHz. The required operating frequencies are marked using vertical lines. The initial design $\boldsymbol{x}^{(0)} = \boldsymbol{s}_I(\boldsymbol{f})$ is marked using a dotted line.

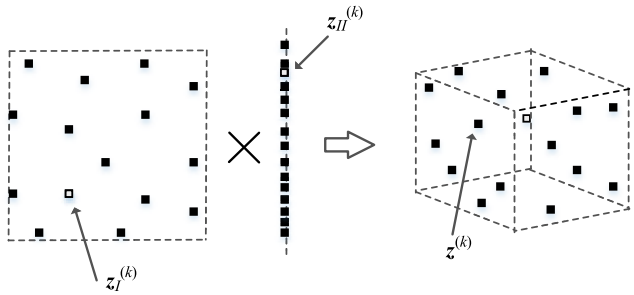

FIGURE 7. Improved design of experiments procedure for the nested kriging framework [70]. The picture shows the allocation of the initial data set $\{z^{(k)}\}$ assuming a two dimensional objective space and three-dimensional design space.

TABLE 2. Nested kriging with improved sampling: Modeling results of dual-band dipole antenna of Fig. 8(a).

Number of training samples	Relative RMS Error			Accuracy Improvement: Improved vs. Original Sampling
	Conventional Kriging	Nested Kriging (original sampling; Section II.B)	Nested Kriging (improved sampling [72])	
50	21.7 %	9.9 %	8.3 %	17 %
100	17.3 %	6.4 %	5.5 %	14 %
200	12.6 %	4.4 %	4.1 %	7 %
400	9.3 %	3.8 %	3.6 %	5 %

A. IMPROVED DESIGN OF EXPERIMENTS

The basic sampling procedure for nested kriging has been described in Section II.B. It allows for a uniform distribution of the training data (from the perspective of the objective space F), by means of the mapping H (8). Notwithstanding, the overall data uniformity may not be the most advantageous allocation having in mind a geometry of the surrogate model domain X_S, specifically the fact that X_S is a "thin" set: its tangential dimensions (along $\boldsymbol{s}_I(F)$) are considerably larger than the orthogonal ones, determined by the parameter T, which is typically set between 0.05 and 0.1 [72]. This means that sample uniformity along $\boldsymbol{s}_I(F)$ may be more important for the model predictive power than the overall uniformity.

The work [72] proposed a modified design of experiments procedure, aiming at the improvement of the data set properties in the sense explained above. According to [72], the initial sample set $\{z^{(k)}\}$ in $[0, 1]^n$ is defined as a Cartesian product of two independent LHS-allocated sets $\{z_I^{(k)}\}$ and $\{z_{II}^{(k)}\}$, both of the same cardinality N_B, allocated in the intervals $[0, 1]^N$ and $[0, 1]^{n-N}$, respectively. In particular, we have

$$z^{(k)} = [z_{I.1}^{(k)} \ \ldots \ z_{I.N}^{(k)} \ z_{II.1}^{(k)} \ \ldots \ z_{II.n-N}^{(k)}]^T, \quad k = 1, \ldots, N_B \tag{10}$$

where $z_I^{(k)} = [z_{I.1}^{(k)} \ldots z_{I.n}^{(k)}]^T$, and $z_{II}^{(k)} = [z_{II.1}^{(k)} \ldots z_{II.n-N}^{(k)}]^T$. Figure 7 shows a graphical illustration of $\{z^{(k)}\}$, $\{z_I^{(k)}\}$ and $\{z_{II}^{(k)}\}$.

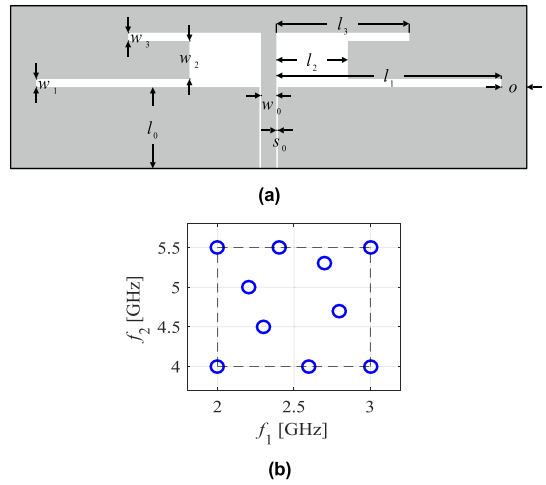

FIGURE 8. Dual-band dipole antenna: (a) antenna geometry [84], (b) allocation of the reference designs.

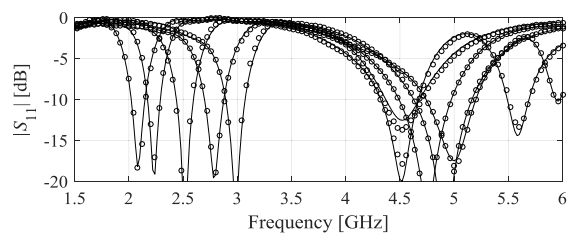

FIGURE 9. Dual-band dipole antenna of Fig. 8(a): reflection characteristics at the selected test designs: EM model (—), nested kriging surrogate with improved sampling constructed using $N = 400$ training samples (o).

For illustration, let us consider a dual-band uniplanar dipole antenna shown in Fig. 8(a) [84]. The antenna geometry is described by six parameters $\boldsymbol{x} = [l_1 \ l_2 \ l_3 \ w_1 \ w_2 \ w_3]^T$, whereas $l_0 = 30$, $w_0 = 3$, $s_0 = 0.15$ and $o = 5$ are fixed (all dimensions in mm). The modeling goal is to set up a surrogate model that covers the following ranges of operating frequencies 2.0 GHz $\leq f_1 \leq$ 3.0 GHz (lower band), and 4.0 GHz $\leq f_2 \leq$ 5.5 GHz (upper band). Figure 8(b) shows the allocation of the reference designs $\boldsymbol{x}^{(j)}, j = 1, \ldots, 10$.

The nested kriging model has been constructed using the training data sets of sizes: sizes from 50 to 400 samples. The thickness parameter was fixed to $T = 0.1$. Table 2 shows the relative RMS error defined as $||\boldsymbol{R}_s(\boldsymbol{x}) - \boldsymbol{R}(\boldsymbol{x})||/||\boldsymbol{R}(\boldsymbol{x})||$, where $\boldsymbol{R}_s(\boldsymbol{x})$ and $\boldsymbol{R}(\boldsymbol{x})$ are the responses of the surrogate model and the EM simulation model at the design $\boldsymbol{x}$, respectively. The errors are averaged over 100 random test samples. For comparison, the table also shows the results for the kriging model constructed within the conventional domain X, and the nested kriging surrogate using the original sampling of Section II.B. Figure 9 shows the antenna responses at the selected test designs.

The results in Table 2 demonstrate noticeable improvement of the model predictive power obtained with the modified sampling scheme. The differences between the original [70] and the design of experiments of [72] are more pronounced

for the smaller data sets (as high as 14 and 17 percent for 100 and 50 training samples, respectively).

B. AUTOMATED ADJUSTMENT OF DOMAIN THICKNESS

The primary control parameter of the nested kriging framework is the domain thickness coefficient T (cf. Section II). Its value is important from the point of view of the model accuracy, the cost of training data acquisition, but also design utility of the model [70]. Decreasing T leads to a significant reduction of the domain volume (e.g., diminishing T by 50 percent when operating in 10-dimensional parameter space and two-dimensional objective space, reduces the model domain volume by almost three orders of magnitude), which has a profound effect on the model predictive power. Numerical studies [70] confirm this observation (see also Table 1, Section II.D). However, reducing T may leave some part of the optimum design manifold $U_F(F)$ outside the domain X_S. This is undesirable from the perspective of design usefulness of the surrogate as the exact optimum is unreachable for some regions of the objective space. A graphical illustration can be found in Fig. 10.

A methodology for automated adjustment of the thickness parameter for the nested kriging was proposed in [73]. The procedure is computationally efficient, based on already available data (i.e., the reference designs), and ensures that the model domain defined with the suggested value of the parameter T contains a majority of the optimum design manifold $U_F(F)$.

The procedure emulates surrogate model optimization, specifically, the behavior of the objective function value U for the optimization runs executed over a range of thickness parameter values. Reaching saturation of U indicates that the model domain contains the manifold $U_F(F)$.

Because the actual surrogate is not available at this stage, the mentioned optimization is carried out using the linear model

$$\boldsymbol{L}(\boldsymbol{z}) = \boldsymbol{R}(\boldsymbol{x}) + \boldsymbol{J}_R(\boldsymbol{x})(\boldsymbol{z} - \boldsymbol{x}) \tag{11}$$

set up at $\boldsymbol{x} \in \boldsymbol{s}_I(F)$. The Jacobian matrix $\boldsymbol{J}_R$ is estimated using finite differentiation. The locations of the testing points $\boldsymbol{x}_T^{(j)}$ correspond to the regions of the objective space where the discrepancy between $\boldsymbol{s}_I(F)$ and $U_F(F)$ is presumably the largest. More specifically, the points $\boldsymbol{x}_T^{(j)}$ are selected as the centers of the simplexes $S^{(j)}$ obtained by the triangulation of the reference designs [73] (cf. Fig. 11).

We denote by $\boldsymbol{b} = [b_1 \ldots b_{n-N}]^T$ a vector of coefficients such that $-1 \leq b_k \leq 1$, $k = 1, \ldots, n-N$, and let $\boldsymbol{f} \in F$. Given the thickness parameter T and $\boldsymbol{x}_T^{(j)} = \boldsymbol{s}_I(\boldsymbol{f}_T^{(j)})$, $j = 1, \ldots, N_S$ (N_S is the cardinality of the simplex set $\{S^{(j)}\}$) the coefficients $a_k(\boldsymbol{f}_T^{(j)})$ are defined using (3). Consider the problem

$$E_j(T) = \min_{\boldsymbol{b},\boldsymbol{f}} U_R\left(\boldsymbol{L}^{(j)}\left(\boldsymbol{s}_I(\boldsymbol{f}) + \sum_{k=1}^{n-N} b_k a_k(\boldsymbol{f}_T^{(j)}) \boldsymbol{v}_n^{(k)}(\boldsymbol{f}_T^{(j)})\right), \boldsymbol{f}_T^{(j)}\right) \tag{12}$$

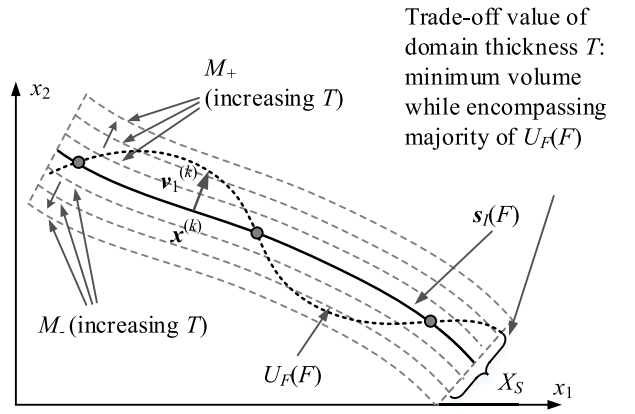

FIGURE 10. Nested kriging framework: the importance of the thickness parameter T. Increasing T enlarges the model domain which allows for encapsulating the optimum design manifold $U_F(F)$. However, more training sample are necessary to construct a reliable surrogate in a larger domain. The optimum trade-off would be the minimum value of T that still allows for incorporating the majority of $U_F(F)$ within the domain.

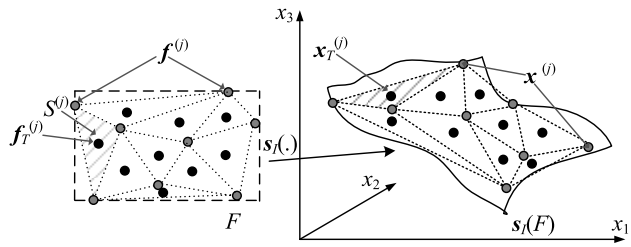

FIGURE 11. Automated adjustment of the thickness parameter T. The picture shows triangulation of the reference designs. The centers $\boldsymbol{f}_T^{(j)}$ of the simplexes $S^{(j)}$ are mapped into the parameter space as $\boldsymbol{x}_T^{(j)} = \boldsymbol{s}_I(\boldsymbol{f}_T^{(j)})$. The vectors $\boldsymbol{x}_T^{(j)}$ are used to determine the domain thickness parameter T.

Here, $\boldsymbol{b} = [0 \ldots 0]^T$ and $\boldsymbol{f} = \boldsymbol{f}_T^{(j)}$ constitute the starting point, whereas U_R is the merit function equivalent to U but with explicit dependence on the system response $\boldsymbol{R}$, i.e., $U_R(\boldsymbol{R}(\boldsymbol{x}), \boldsymbol{f}) = U(\boldsymbol{x}, \boldsymbol{f})$. Observe that $\left[\boldsymbol{s}_I(\boldsymbol{f}) + \sum_{k=1}^{n-N} b_k a_k(\boldsymbol{f}_T^{(j)}) \boldsymbol{v}_n^{(k)}(\boldsymbol{f}_T^{(j)})\right] - \boldsymbol{s}_I(\boldsymbol{f}_T^{(j)})$ represents a deviation from the starting point $\boldsymbol{x}_T^{(j)} = \boldsymbol{s}_I(\boldsymbol{f}_T^{(j)})$, with $\boldsymbol{s}_I(\boldsymbol{f}) - \boldsymbol{s}_I(\boldsymbol{f}_T^{(j)})$ and $\sum_{k=1}^{n-N} b_k a_k(\boldsymbol{f}_T^{(j)}) \boldsymbol{v}_n^{(k)}(\boldsymbol{f}_T^{(j)})$ being shifts along the manifold $\boldsymbol{s}_I(F)$ and towards the normal vectors $\boldsymbol{v}_n^{(k)}$, respectively; $\boldsymbol{L}^{(j)}$ is of the form (11), established at $\boldsymbol{x}_T^{(j)}$.

For a sequence $T_1 = 0 < T_2 < \ldots < T_{NT}$ (T_{NT} is set to ensure that $U_F(F) \subset X_S$ for X_S defined using T_{NT}; in practice, $T_{NT} = 0.2$ is sufficient in most practical cases), the sequence $E_j(T_k)$ obtained using (12) will be decreasing and converging to $E_j(T_{NT})$. Let

$$E_{N.k}^{(j)} = \frac{E_j(T_k) - \min\{k : E_j(T_k)\}}{\max\{k : E_j(T_k)\} - \min\{k : E_j(T_k)\}} \tag{13}$$

and

$$E_{aver.k} = \frac{1}{N_S} \sum_{j=1}^{N_S} E_{N.k}^{(j)} \tag{14}$$

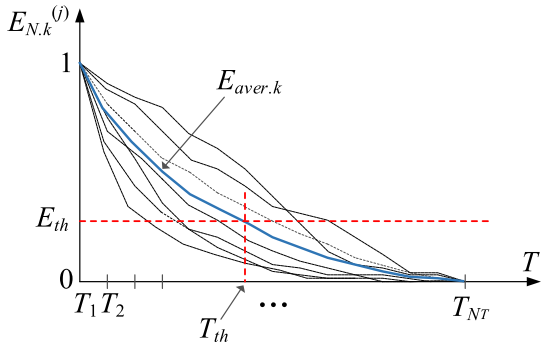

FIGURE 12. Normalized sequences $E_{N.k}^{(j)}$ of (13) and the average sequence $E_{aver.k}$ of (14). The recommended value T_{th} of T is based on the threshold E_{th} of the normalized objective function.

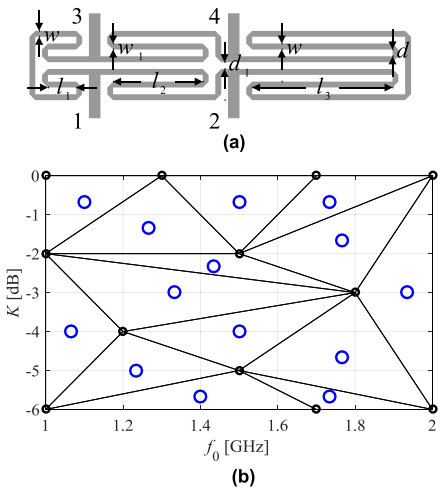

FIGURE 13. Compact microstrip rat-race coupler (RRC) [73]: (a) circuit geometry, (b) reference designs (small circles), their triangulation, and the simplex centers $x_T^{(j)}$ (large circles) used to estimate the thickness parameter T.

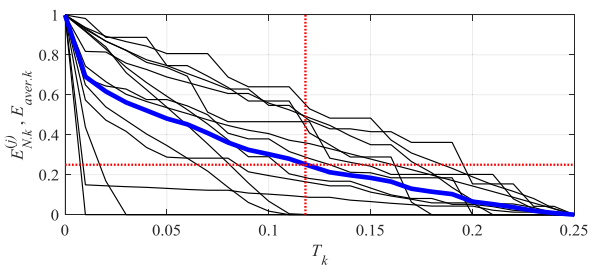

FIGURE 14. Rat-race coupler: normalized objective value sequences $E_{N.k}^{(j)}$ (thin lines) and the average sequence $E_{aver.k}$ (thick line). The recommended value of T (obtained for $E_{th} = 0.25$) is $T_{th} = 0.115$.

be the normalized sequences and their average over $j = 1, \ldots, N_S$. The recommended value T_{th}, is assigned as the one corresponding to the average value of the normalized objective equal to the threshold level E_{th} (cf. Fig. 12). In [73], $E_{th} = 0.25$ was used. The described procedure is approximate but computationally efficient as it only requires $N_S(n+1) \approx p(n+1)$ EM simulations (the number of simplexes $S^{(i)}$ is typically close to the number p of the reference designs).

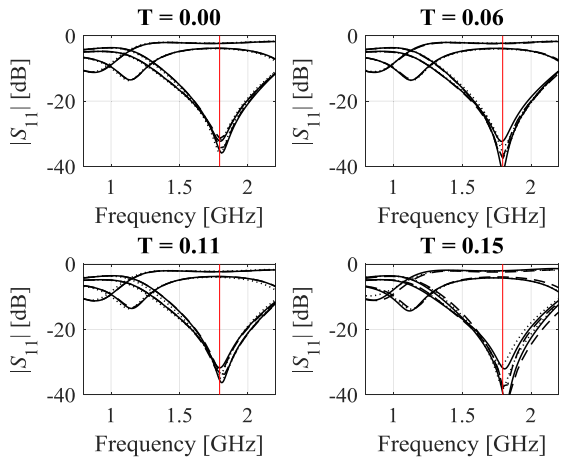

FIGURE 15. Rat-race coupler: initial design (· · ··), surrogate model at the optimized design (- - -), and EM-simulated response at the optimized design (—) for nested-kriging surrogates constructed with the domain thickness parameters $T = 0$, $T = 0.06$, $T = 0.11$ (recommended value), and $T = 0.15$, shown for a selected target objective vector. The recommended value gives a good compromise between the surrogate model prediction and further agreement with the EM simulation results.

For the sake of illustration, let us consider a compact rat-race coupler (RRC) [73] shown in Fig. 13(a), implemented on RF-35 substrate ($\varepsilon_r = 3.5$, $h = 0.762$ mm). The geometry parameters of the structure are $\boldsymbol{x} = [l_1\ l_2\ l_3\ d\ w\ w_1]^T$; other dimensions are $d_1 = d + |w - w_1|$, $d = 1.0$, $w_0 = 1.7$, and $l_0 = 15$ fixed (all in mm). The computational model $\boldsymbol{R}$ is implemented in CST Microwave Studio. The figures of interest are the operating frequency f_0 and the power split ratio K. The goal is to construct the surrogate covering the objective space defined by 1 GHz $\leq f \leq$ 2 GHz and –6 dB $\leq K \leq$ 0 dB. The details concerning the reference designs and conventional parameter space can be found in [73].

The thickness parameter has been estimated using the procedure described above (see also Fig. 13(b)). The recommended value $T_{th} = 0.115$, cf. Fig. 14. For verification, the nested kriging surrogate was constructed for T from 0.0 to 0.15 (with the step of 0.01). The models were optimized for a number of objective vectors $\boldsymbol{f}$ (the points $\boldsymbol{f}_T^{(j)}$ supplemented by random locations, 50 points in total). The results, gathered in Table 3 indicate saturation starting at around $T = 0.10$, which agrees well with T_{th}.

For additional validation, the models obtained for $T = 0.0$, 0.06, 0.11, and 0.15 have been investigated in more detail. As shown in Fig. 15, the predictions provided by the surrogate agree well with EM simulation results for the models constructed with $T = 0.0$ and 0.6, and it is slightly worse for $T = 0.11$. For $T = 0.15$, the discrepancies between the surrogate and EM simulation become noticeable, i.e., reliability of the optimization process is degraded. The models constructed in larger domains allow for yielding designs that exhibit improved objective function levels. The recommended value of T provides a reasonable compromise between the quality of surrogate prediction and the achievable optimum design. Also, using T slightly smaller than the recommended value seems to be a good option.

TABLE 3. Nested kriging with automated adjustment of domain thickness: Surrogates and their optimization results for rat-race coupler of. Fig. 13(a).

Thickness parameter T	Relative RMS error#	Model optimization: average objective function value$
0.00	0.7 %	–23.8 dB
0.01	1.2 %	–26.2 dB
0.02	1.7 %	–26.8 dB
0.03	2.2 %	–27.3 dB
0.04	2.8 %	–27.7 dB
0.05	3.3 %	–28.0 dB
0.06	4.0 %	–28.1 dB
0.07	4.6 %	–28.2 dB
0.08	5.1 %	–28.4 dB
0.09	5.1 %	–28.6 dB
0.10	6.1 %	–28.9 dB
0.11	6.6 %	–29.0 dB
0.12	7.2 %	–29.0 dB
0.13	7.7 %	–29.2 dB
0.14	8.3 %	–29.3 dB
0.15	8.9 %	–29.3 dB

Model accuracy estimated using the split-sample method based on 100 random samples. The table provides relative error $||R(x) - R_s(x)||/||R(x)||$ averaged over the testing set. Surrogate model set up with N_B = 800 samples.

$ Surrogate model optimized within the domain X_S. The displayed value is the average over fifty initial designs including the simplex centers $x_r^{(j)}$ and additional random points.

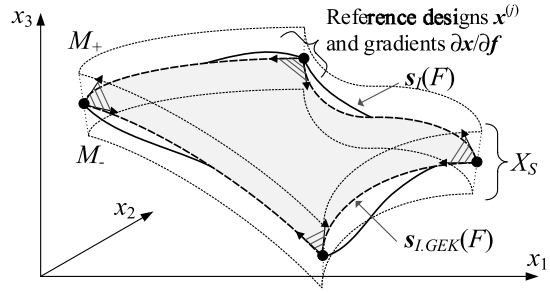

FIGURE 16. Conceptual illustration of the sensitivity-based first-level model for the nested kriging framework. Shown are the image of the GEK-based model $s_{I.GEK}(F)$ and the domain X_S defined as the extension of $s_{I.GEK}(F)$. Here, the first-level model is defined using the corner reference designs $x^{(j)}$ only and their corresponding sensitivities $\partial x/\partial f = \partial U_F(f^{(j)})/\partial f$ marked using arrows and gray shading.

TABLE 4. GEK-based nested kriging: Modeling results for impedance matching transformer of Fig. 17(a).

Number of Training Samples	Relative RMS Error			
	Conventional Kriging Model	Conventional RBF	Conventional Nested Kriging Model [71]	GEK-based Nested Kriging Model [75]
50	49.1 %	56.2 %	17.3 %	14.6 %
100	31.1 %	33.0 %	13.9 %	9.3 %
200	25.9 %	27.5 %	10.3 %	7.2 %
400	20.4 %	23.1 %	7.4 %	7.1 %
800	15.7 %	16.8 %	6.1 %	5.1 %

C. NESTED KRIGING WITH GRADIENT-BASED FIRST-LEVEL SURROGATE

One of the practical issues of the nested kriging but also other performance-driven modeling methods is a high initial cost related to acquisition of the reference designs. The number of the reference designs rapidly increases with the dimensionality of the objective space and obtaining each one of them required a separate optimization run. In [74] and [75], a technique for reducing the number of reference points needed to construct the first-level model $\boldsymbol{s}_I(\boldsymbol{f})$ has been proposed using the gradient enhanced kriging (GEK) method [85].

The model $\boldsymbol{s}_I(\boldsymbol{f})$ is an inverse surrogate identified using the pairs $\{\boldsymbol{f}^{(j)}, \boldsymbol{x}^{(j)}\}$, $j = 1, \ldots, p$, where $\boldsymbol{f}^{(j)}$ are the objective vectors and $\boldsymbol{x}^{(j)}$ are the parameter vectors optimized in (1). Because $\boldsymbol{s}_I(F)$ is a low-dimensional object, gradient-enhanced kriging is suitable to limit p by incorporating the sensitivity data $\boldsymbol{J}^x(\boldsymbol{f}) = \partial \boldsymbol{x}/\partial \boldsymbol{f} = \partial U_F(\boldsymbol{f})/\partial \boldsymbol{f}$. The entries J_{jkx} of $\boldsymbol{J}^x(\boldsymbol{f})$ are the partial derivatives of the (optimized) parameters x_j with respect to f_k. These can be estimated using the system response sensitivities already known as a by-product of solving (1). Let $\boldsymbol{R}(\boldsymbol{x})$ be the response of the EM model of the system at hand and $\boldsymbol{J}(\boldsymbol{x})$ be its Jacobian matrix at $\boldsymbol{x}$. Further, let $\boldsymbol{d} = [d_1 \ldots d_N]^T$ be a vector of perturbations of the performance figures. We first find the perturbed designs $\boldsymbol{x}^{(j.k)}$ corresponding to $[f_1^{(j)} \ldots f_k^{(j)} + d_k \ldots f_N^{(j)}]^T$, as

$$\boldsymbol{x}^{(j.k)} = \arg\min_{\boldsymbol{x}} U_L(\boldsymbol{x}; f_1^{(j)}, \ldots, f_k^{(j)} + d_k, f_N^{(j)}) \tag{15}$$

The U_L is based on the first-order model $\boldsymbol{R}(\boldsymbol{x}) = \boldsymbol{R}(\boldsymbol{x}^{(j)}) + \boldsymbol{J}(\boldsymbol{x}^{(j)}) \cdot (\boldsymbol{x} - \boldsymbol{x}^{(j)})$ to ensure low cost of solving (15). The actual figures interest $[f_1^{(j.k)} \ldots f_N^{(j.k)}]^T$ at $\boldsymbol{x}^{(j.k)}$ are extracted from $\boldsymbol{R}(\boldsymbol{x}^{(j.k)})$. As d_k are small, we have

$$x_l^{(j.k)} \approx x_l^{(j)} + \sum_{r=1}^{N} J_{lr}^x(\boldsymbol{x}^{(j)})[f_r^{(j.k)} - f_r^{(j)}] \tag{16}$$

The matrix form of (16) is $\boldsymbol{X} = \boldsymbol{J}^x \boldsymbol{F}$, where $\boldsymbol{X} = [\boldsymbol{x}^{(j.1)} - \boldsymbol{x}^{(j)} \ldots \boldsymbol{x}^{(j.N)} - \boldsymbol{x}^{(j)}]$ and $\boldsymbol{F} = [f^{(j.l)} - x^{(j)}]_{k,l=1,\ldots,N}$. If $\boldsymbol{F}$ is nonsingular, which is typically the case as off-diagonal elements are normally small, then we get

$$\boldsymbol{J}^x = \boldsymbol{X}\boldsymbol{F}^{-1} \tag{17}$$

Using $\{\boldsymbol{f}^{(j)}, \boldsymbol{x}^{(j)}, \boldsymbol{J}^x(\boldsymbol{f}^{(j)})\}$, $j = 1, \ldots, p$, as the training set, the first-level model can be constructed using GEK [85]. The benefit is a significantly smaller number of data samples required to yield the model as compared to the derivative-free version. The remaining components of the nested kriging remain unchanged as compared to the formulation in Section II. A graphical illustration of the sensitivity-based first-level model can be found in Fig. 16.

The benefits of the sensitivity-based modeling are demonstrated using the 50-to-100 Ohm impedance matching transformer shown in Fig. 17(b). The designable variables are $\boldsymbol{x} = [l_{1.1}\ l_{1.2}\ w_{1.1}\ w_{1.2}\ w_{1.0}\ l_{2.1}\ l_{2.2}\ w_{2.1}\ w_{2.2}\ w_{2.0}\ l_{3.1}\ l_{3.2}\ w_{3.1}\ w_{3.2}\ w_{3.0}]^T$. The objective space is defined by the following

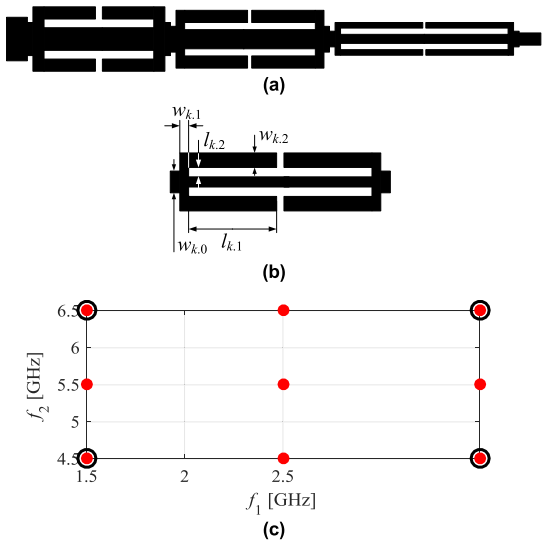

FIGURE 17. CMRC-based three-section impedance transformer: (a) compact cell (CMRC), (b) transformer geometry [71], (c) reference designs for the conventional nested-kriging technique (solid circles) (9 reference points) and the gradient-enhanced technique (o) (only 4 reference points in the objective space corners).

ranges of operating bands $[f_1 f_2]$ (defined by $|S_{11}| \leq -20$ dB): with 1.5 GHz $\leq f_1 \leq$ 3.5 GHz, and 4.5 GHz $\leq f_2 \leq$ 6.5 GHz.

The allocation of the reference designs for the original and sensitivity-based nested kriging are shown in Fig. 17(c). The first-level surrogates rendered by both frameworks are in good agreement (cf. Fig. 18). Note that the GEK-based model requires only four reference designs versus nine for the original version.

The modelling results and comparisons with the benchmark techniques can be found in Table 4 (see also Fig. 19). It should be emphasized that despite the reduced number of reference designs, the accuracy of the gradient-enhanced surrogates is slightly better than that of the basic version of the nested kriging technique, let alone the conventional methods.

D. NESTED KRIGING WITH RESPONSE FEATURES

The response feature technology [86], [87], was introduced to speed up the simulation-based design procedures by exploring the particular structure of the systems outputs (primarily, the frequency characteristics). It capitalizes on the observation that the feature point coordinates are typically only weakly nonlinear (as functions of the design parameters) as compared to the original outputs. The characteristic points (features) are selected to be sufficient for evaluating the design quality. In [76], an incorporation of the response feature approach into the nested kriging framework has been proposed for a particular case of multi-band antennas. The concept is briefly recalled and illustrated in this section.

When handling input characteristics of multi-band antennas, an appropriate choice of the feature points would be the frequency locations of the antenna resonances and the points corresponding to −10 dB level of reflection. These points can be extracted from the EM simulation results and used

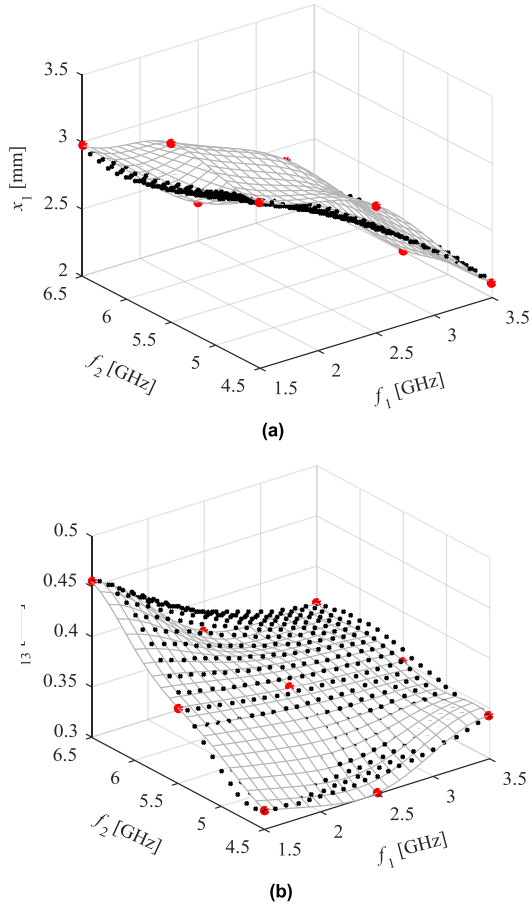

FIGURE 18. First-level models $s_I(f) : F \rightarrow X$ for selected design variables of the transformer of Fig. 17(b) as functions of the performance figures: nested kriging (mesh surface) and GEK-based (black circles); red circles indicate reference designs utilized by the original nested kriging technique (GEK-based first level model utilizes four designs in the corners of the space F).

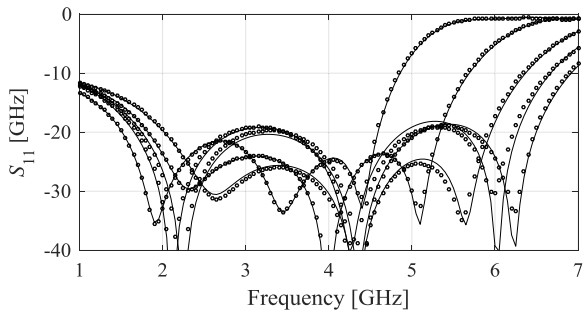

FIGURE 19. Impedance matching transformer: reflection characteristics at the selected test designs: EM simulation model (—), the GEK-based surrogate obtained using $N = 400$ training samples (o).

to allocate the resonances at the required operating frequencies and/or optimize the antenna for maximum bandwidth (see Fig. 20).

For the sake of explanation, we denote the feature points referring to p antenna resonances as $\boldsymbol{R}_F(\boldsymbol{x}) = [f_1(\boldsymbol{x})\, f_2(\boldsymbol{x}) \ldots f_p(\boldsymbol{x})\; l_1(\boldsymbol{x})\; l_2(\boldsymbol{x}) \ldots l_p(\boldsymbol{x})]^T$, where f_k and l_k stand for their frequency and level coordinates, $k = 1, \ldots, p$, respectively.

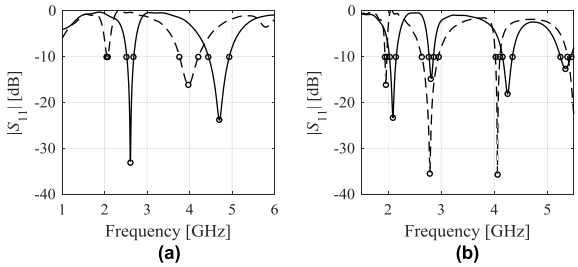

FIGURE 20. Exemplary reflection responses and the feature points (here, corresponding to antenna resonances and −10 dB reflection levels) for: (a) dual-band antenna, (b) triple-band antenna.

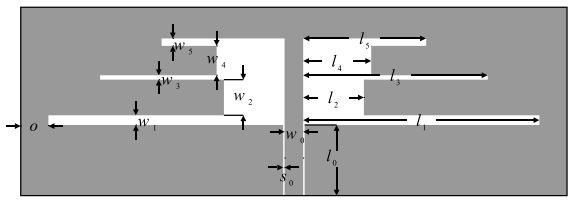

FIGURE 21. Geometry of the triple-band dipole antenna [83].

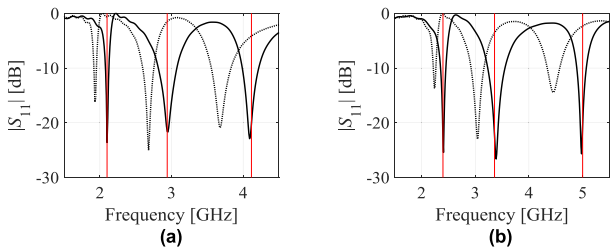

FIGURE 22. Triple-band dipole antenna: optimization using feature-based nested kriging: EM-simulated responses at the initial designs (. . . . .) obtained from the surrogate, and optimized responses (–). Target operating frequencies marked using vertical lines: (a) $f_1 = 2.1$ GHz, $k_1 = 1.4$, $k_2 = 1.4$ ($f_2 = 2.94$ GHz, $f_3 = 4.12$ GHz), (b) $f_1 = 2.4$ GHz, $k_1 = 1.4$, $k_2 = 1.5$ ($f_2 = 3.36$ GHz, $f_3 = 5.04$ GHz).

In feature-based nested kriging [76], the first-level surrogate and the domain definition are the same as in Section II. The training set for the final surrogate is $\{\boldsymbol{x}_B^{(k)}, \boldsymbol{R}_F(\boldsymbol{x}_B^{(k)})\}_{k=1,\ldots,NB}$. If the design objectives can be quantified using the selected feature points, modelling of $\boldsymbol{R}_F$ rather than $\boldsymbol{R}$ does not lead to any loss of information from the design perspective.

For illustration, consider a triple-band dipole antenna shown in Fig. 21 [83]. The antenna is implemented on RO4350 substrate ($\varepsilon_r = 3.48$, $h = 0.762$ mm) and fed by a coplanar waveguide. The geometry parameters are: $\boldsymbol{x} = [l_1\ l_2\ l_3\ l_4\ l_5\ w_1\ w_2\ w_3\ w_4\ w_5]^T$; where $l_0 = 30$, $w_0 = 3$, $s_0 = 0.15$ and $o = 5$ are fixed (all dimensions in mm). The computational model is simulated in CST Microwave Studio and with its time-domain solver. The surrogate model should be valid for the operating frequencies f_k, $k = 1, 2, 3$, $f_2 = f_1k_1$, $f_3 = f_2k_2$, within the following ranges: 1.5 GHz $\leq f_1 \leq$ 2.5 GHz, $1.2 \leq k_1 \leq 1.6$, and $1.2 \leq k_2 \leq 1.6$. The details concerning the reference designs and the conventional parameter space can be found in [76].

TABLE 5. Feature-based nested kriging: Modeling results for triple-band antenna of Fig. 21.

Number of Training Samples	Relative RMS Error			
	Conventional Kriging Model	Conventional RBF	Nested Kriging Model [70]	Feature-based Nested Kriging [77]
20	28.5 %	30.1 %	38.9 %	2.65 %
50	22.7 %	23.5 %	16.0 %	0.25 %
100	19.9 %	19.8 %	11.2 %	0.22 %
200	18.6 %	19.2 %	9.9 %	0.19 %
400	17.2 %	18.8 %	9.7 %	0.14 %
800	16.8 %	17.4 %	7.8 %	0.20 %

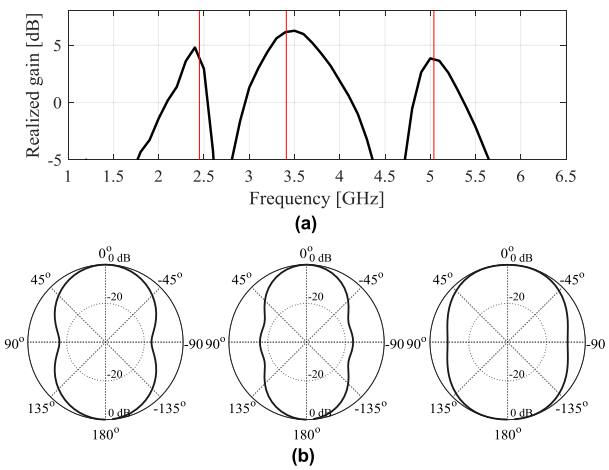

FIGURE 23. Triple-band dipole antenna: simulated characteristics at the design shown in Fig. 26(b): (a) realized gain, (b) H-plane radiation patterns at 2.45 GHz, 3.36 GHz, and 5.04 GHz, respectively. The target operating frequencies shown using vertical lines.

Table 5 gathers the numerical results (average relative RMS calculated based on 100 independent random test points) for several modeling scenarios. Modelling the feature-point coordinates instead of the complete responses allows for achieving a considerably better predictive power of the surrogate. Application examples shown in Fig. 22 indicate that this has no detrimental effects on the model design utility. Figure 23 shows the realized gain as well as radiation patterns of the antenna of Fig. 21 at the design of Fig. 22(b).

E. NESTED KRIGING WITH VARIABLE-FIDELITY MODELS

The involvement of variable-fidelity EM simulations is a natural way of reducing the cost of training data acquisition when constructing the surrogate. One of the popular approaches to blend the low- and high-fidelity simulation data is co-kriging [64]. In the context of modeling of high-frequency structures, it is more suitable for handling components that exhibit wideband characteristics where the discrepancies between the models of various fidelities are mostly vertical (i.e., concern the response levels rather than frequency shifts). In [83] and [88], the nested kriging was combined with co-kriging, which is rather straightforward: the first-level model

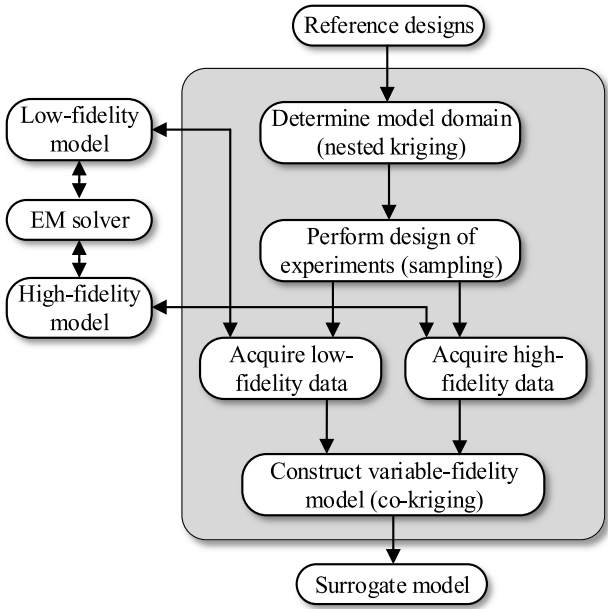

FIGURE 24. Flow diagram of nested kriging with variable-fidelity EM simulations and co-kriging.

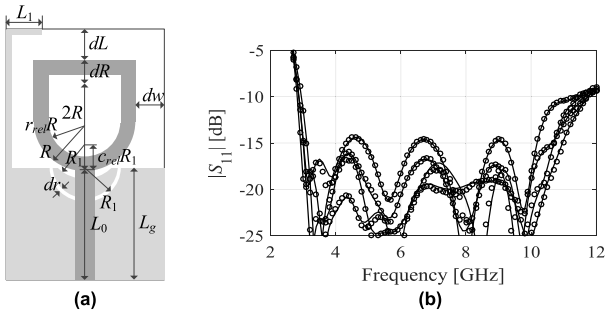

FIGURE 25. Wideband monopole antenna [89]: (a) geometry (ground plane shown using light gray shade), (b) reflection responses at the selected test designs: EM model (–), nested co-kriging surrogate with Nf = 50 and Nc = 400 (o).

is constructed in a traditional manner (cf. Section II), whereas the final surrogate is a co-kriging one, using a limited number of high-fidelity data. Figure 24 shows the flow diagram of the modeling procedure.

For illustration, consider an ultra-wideband monopole antenna of Fig. 25(a) [89]. The variables are $\boldsymbol{x} = [L_0\ dR\ Rr_{rel}\ dL\ dw\ L_gL_1R_1\ dr\ c_{rel}]^T$. The antenna is supposed to operate from 3.1 GHz to 10.6 GHz. The EM models are implemented in CST: low-fidelity model $\boldsymbol{R}_c$ (~380,000 mesh cells, simulation time 56 seconds), high-fidelity model $\boldsymbol{R}_f$ (~1,800,000 cells, 400 seconds). Both models incorporate the SMA connectors.

The surrogate model is supposed to be valid within the objective space defined by the parameters of the substrate the antenna is implemented on: permittivity $2.0 \leq \varepsilon_r \leq 5.0$ and height 0.5 mm $\leq h \leq$ 1.5 mm. The details concerning the reference designs can be found in [83].

The nested co-kriging model has been constructed using various numbers of high- and low-fidelity samples N_f and N_c: $N_f = 20$ and $N_c = 400$, $N_f = 50$ and $N_c = 400$, $N_f = 100$ and $N_c = 400$, as well as $N_f = 50$ and $N_c = 800$. The numerical results are gathered in Table 6 (see also Fig. 25(b)). It can be observed that the accuracy of the nested co-kriging is comparable to that of the high-fidelity nested kriging obtained using 400 and 800 samples. However, the cost of training data acquisition is lower than for the high-fidelity-only nested kriging. Depending on the setup (i.e., N_f and N_c) it is just between 76 and 162 equivalent high-fidelity model evaluations.

TABLE 6. Nested kriging with variable-fidelity models: Modeling results for wideband monopole antenna of Fig. 25(a).

Number of training samples	Relative RMS error						
	Conventional models		Nested kriging model	Nested co-kriging model [84]*			
	kriging	RBF		$N_f = 20$ $N_c = 400$	$N_f = 50$ $N_c = 400$	$N_f = 100$ $N_c = 400$	$N_f = 50$ $N_c = 800$
50	62.5 %	65.1 %	10.8 %				
100	48.5 %	51.2 %	7.9 %				
200	37.3 %	38.7 %	6.4 %	7.6 % [76#]	5.2 % [106#]	4.3 % [156#]	5.0 % [162#]
400	32.4 %	33.5 %	5.9 %				
800	22.7 %	24.6 %	5.4 %				

*N_f and N_c stand for the number of high- and low-fidelity samples, respectively.
#The number is brackets is the total equivalent number of R_f samples used to set up the surrogate (calculated as $N_f + N_c/m$ where m is the time evaluation ratio between R_f and R_c).

F. NESTED KRIGING WITH DOMAIN DIMENSIONALITY REDUCTION

As explained in Section II, the nested kriging framework attempts to construct the surrogate model in the vicinity of the optimum design manifold $U_F(F)$, using the set of reference designs $\boldsymbol{x}^{(j)} = U_F(\boldsymbol{f}^{(j)}) = [x_1^{(j)} \ldots x_n^{(j)}]^T, j = 1, \ldots, p$, where $\boldsymbol{f}^{(j)} = [f_1^{(j)} \ldots f_N^{(j)}] \in F$.

The reference designs provide information about $U_F(F)$ but also about correlations between optimum parameter sets. This has been explored in [77], where the nested kriging with dimensionality reduction was introduced using the spectral analysis of $\{\boldsymbol{x}^{(k)}\}$. Given a center of gravity of $\{\boldsymbol{x}^{(k)}\}$

$$\boldsymbol{x}_m = \frac{1}{p}\sum_{k=1}^{p} \boldsymbol{x}(k) \tag{18}$$

the covariance matrix $\boldsymbol{S}_p$ of $\{\boldsymbol{x}^{(k)}\}$ can be defined as

$$\boldsymbol{S}_p = \frac{1}{p-1}\sum_{k=1}^{p} (\boldsymbol{x}^{(k)} - \boldsymbol{x}_m)(\boldsymbol{x}^{(k)} - \boldsymbol{x}_m)^T \tag{19}$$

The eigenvectors $\boldsymbol{a}_k$, $k = 1, \ldots, n$ of $\boldsymbol{S}_p$ (principal components of $\{\boldsymbol{x}^{(k)}\}$) [90] determine the directions of the most important correlations between the optimum system parameters within F. The eigenvalues λ_k, representing the variance of $\{\boldsymbol{x}^{(k)}\}$ in the eigenspace, are assumed to be ordered, i.e., $\lambda_1 \geq \lambda_2 \geq \ldots \geq \lambda_n \geq 0$.

The first-level surrogate $\boldsymbol{s}_I(\boldsymbol{f})$: $F \rightarrow X$, is constructed as in Section II, using $\{\boldsymbol{f}^{(j)}, \boldsymbol{x}^{(j)}\}, j = 1, \ldots, p$, as the training set.

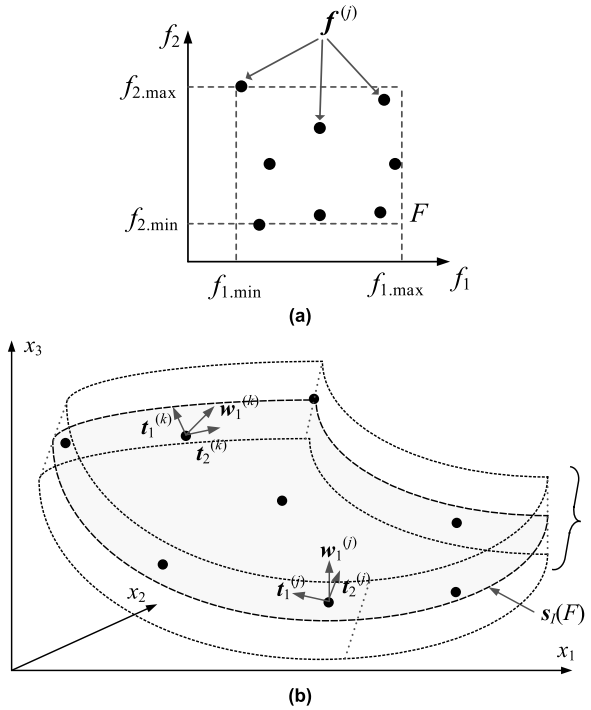

FIGURE 26. Basic components of nested kriging with dimensionality reduction: (a) objective space F, (b) reference designs and the first-level model image $s_I(F)$. Also shown are two exemplary points $s_I(f)$ along with their corresponding tangent vectors t_1 and t_2 and the normal vector w_1 obtained as in (22).

In nested kriging, the model domain is defined by extending $s_I(F)$ towards vectors $\{v_n^{(k)}(f)\}$, $k = 1, \ldots, n - N$, that are normal to $s_I(F)$ at all $f \in F$ [70]. The extension amount is controlled by the thickness parameter T. The domain dimensionality n is the same as the dimensionality of the original parameter space X.

In [77], the domain was defined through selective extension, realized with $K \leq n$ normal vectors, determined from the principal components a_k. For a non-trivial extension, one needs $K > N$. We denote by $t_j(f)$, $j = 1, \ldots, N$, the vectors tangent to $s_I(F)$ at f. The representation of $\{t_j(f)\}_{j=1,\ldots,N}$ with respect to $\{a_k\}_{k=1,\ldots,K}$, can be found as

$$\left[\bar{t}_1(f) \ \ldots \ \bar{t}_N(f)\right] = A_K^T \left[t_1(f) \ \ldots \ t_N(f)\right] \tag{20}$$

where $A_K = [a_1 \ \ldots \ a_K]$; and $\bar{t}_j(f)$ are $K \times 1$ vectors. Let $T(f)$ be a complement of $\left[\bar{t}_1(f) \ \ldots \ \bar{t}_N(f)\right]$ to a square $K \times K$ matrix $T(f) = \left[\bar{t}_1(f) \ \ldots \ \bar{t}_N(f) \ e_{N+1} \ e_{N+2} \ \ldots \ e_K\right]$, where $e_j = [0 \ldots 010 \ldots 0]^T$ with 1 at the jth position. The matrix $T_{GS}(f)$ of K orthonormal vectors

$$T_{GS}(f) = \left[\tilde{t}_1(f) \ \ldots \ \tilde{t}_N(f) \ w_1(f) \ \ldots \ w_{K-N}(f)\right] \tag{21}$$

is then obtained from $T(f)$ using a Gram-Schmidt procedure [91]. Among these, the vectors $w_j(f)$, $j = 1, \ldots, K - N$, will be used to realize the orthogonal extension of $s_I(F)$. The number of principal components employed in the procedure (in practice, $K - N = 1$ or 2) should be decided upon based on the eigenvalue analysis.

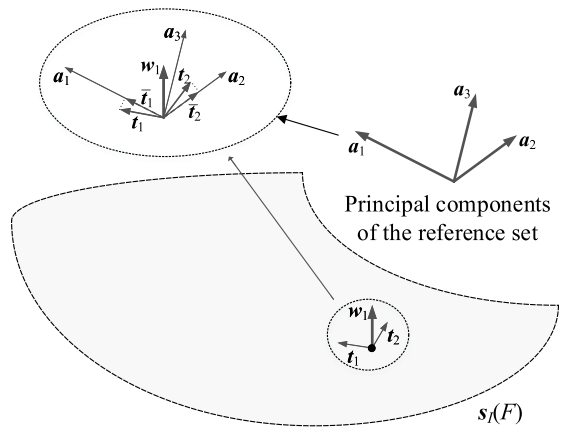

FIGURE 27. Construction of the extension basis $\{w_j(f)\}$ of (21). The picture shows the set $s_I(F)$, a selected reference design, its corresponding tangent vectors $\{t_j\}$, and zoom onto the construction procedure shown in the inset.

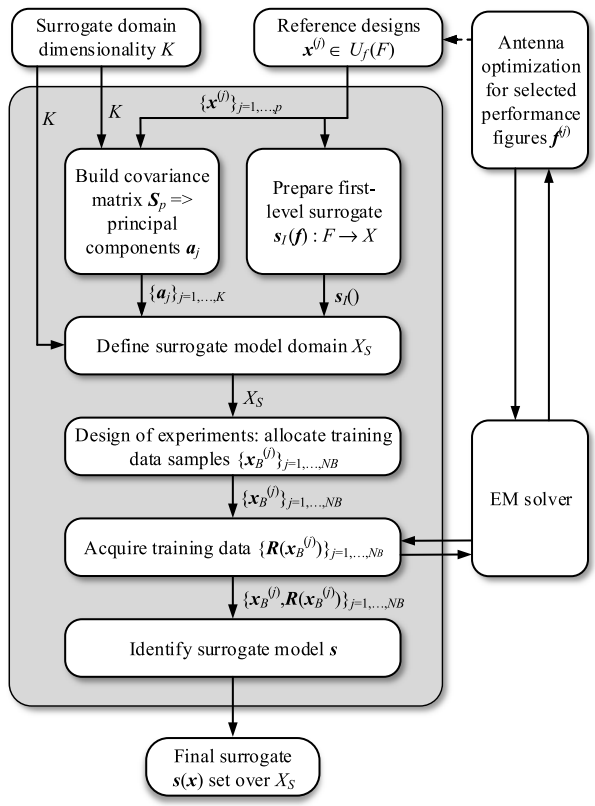

FIGURE 28. Flow diagram of the nested kriging with dimensionality reduction.

The surrogate model domain X_S is defined as

$$X_S = \left\{ \begin{array}{c} x = s_I(f) + T \sum_{k=1}^{K-N} \lambda_k w_n^{(k)}(f) : f \in F, \\ -1 \leq \lambda_k \leq 1, \ k = 1, \ldots, K - N \end{array} \right\} \tag{22}$$

The thickness parameter T is similar to that used by the nested kriging framework and it is set to be a fraction (five to ten percent) of the reference set extent towards the first principal component and also takes into account the relationships between the eigenvalues λ_k. The dimensionality of X_S is K.

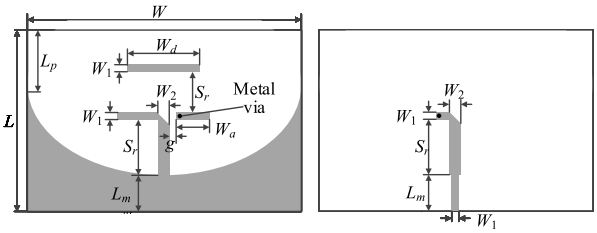

FIGURE 29. Quasi-Yagi antenna [92]: (a) top layer, (b) bottom layer.

Figures 26 and 27 show the basic components of the modeling framework.

Having the domain X_S defined as in (22), the final surrogate $\boldsymbol{s}(\boldsymbol{x})$ is constructed using kriging interpolation. The training data is denoted the same way as in Section II, i.e., $\{\boldsymbol{x}_B^{(k)}, \boldsymbol{R}(\boldsymbol{x}_B^{(k)})\}_{k=1,\ldots,NB}$, where $\boldsymbol{x}_B^{(k)} \in X_S$ are uniformly allocated samples and $\boldsymbol{R}(\boldsymbol{x})$ is the response of the EM-simulation model of the system at hand at $\boldsymbol{x}$.

The details concerning design of experiments and surrogate model optimization can be found in [77]. The flow diagram of the modeling process has been shown in Fig. 28. The overall benefits of the presented approach are the same as for the basic version of the nested kriging. Additional advantages come from dimensionality reduction and include further improvement of the predictive power and improved scalability as a function of the training data set size.

Let us consider a verification case, which is a quasi-Yagi antenna with a parabolic reflector [92] shown in Fig. 29, and described by ten parameters $\boldsymbol{x} = [W\ L\ L_m\ L_p\ S_d\ S_r\ W_2 W_a\ W_d\ g]^T$ (all dimensions in mm). The antenna is implemented on 1.5-mm-thick substrate. The feed line width W_1 is computed for a given substrate permittivity ε_r to ensure 50-ohm input impedance. The permittivity is as an operating condition and a part of the objective space F. The EM model is simulated in CST Microwave Studio.

The modeling goal is to render the surrogate valid for the following ranges of operating frequency and ε_r: 2.5 GHz $\leq f_0 \leq$ 5.0 GHz and $2.5 \leq \varepsilon_r \leq 4.5$. The antenna characteristics of interest are reflection and realized gain. A few comments are necessary concerning the design optimality. It is understood, for a given center frequency f_0, in the following sense: (i) ensure at least 8-percent fractional bandwidth (symmetric w.r.t. f_0), assuming a given substrate permittivity ε_r, (ii) maximize the average realized gain within the same 8-percent bandwidth. This can be formalized as minimization of the following objective function

$$U(\boldsymbol{x},\boldsymbol{f}) = U(\boldsymbol{x}, [f_0\ \varepsilon_r]^T) = -(f_0 B)^{-1} \int_{f_0(1-B/2)}^{f_0(1+B/2)} G(\boldsymbol{x}, f)df + \beta c(\boldsymbol{x}) \quad (23)$$

In (23), $G(\boldsymbol{x}, f)$ denotes the realized gain at the design $\boldsymbol{x}$ and frequency f; $\beta c(\boldsymbol{x})$ stands for the penalty term with β being a penalty coefficient and c being a penalty function. The function c quantifies violation of the constraint $|S_{11}| \leq -10$ dB and it is defined as $c(\boldsymbol{x}) = \max\{\max\{f_0(1-B/2) \leq f \leq f_0(1+B/2) : |S_{11}(\boldsymbol{x}, f)| + 10\}, 0\}^2$. There are eight

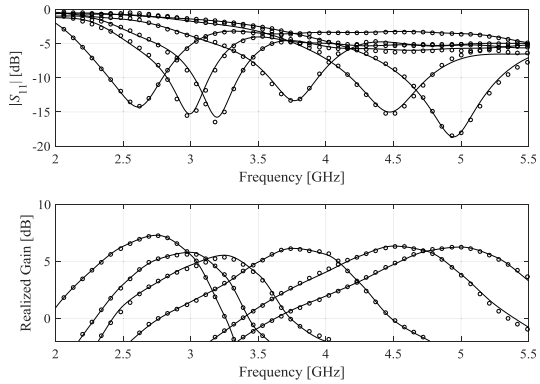

FIGURE 30. Quasi-Yagi antenna: reflection characteristics at the selected test designs: EM simulation (—), surrogate model with dimensionality reduction set up using $K = 4$ and $N = 200$ (o).

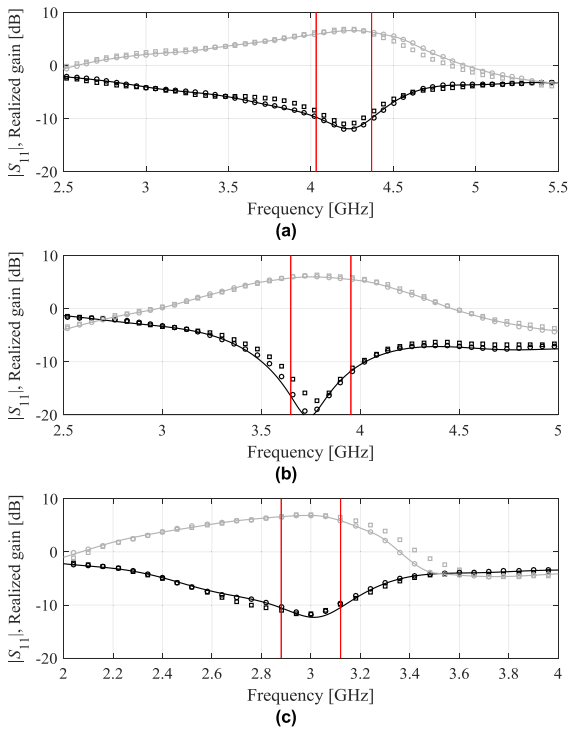

FIGURE 31. Quasi-Yagi antenna: application case studies. Shown are: the nested-kriging surrogate with dimensionality reduction (o), the nested kriging model [70] (□) and EM simulation at the design obtained through optimization of the surrogate (—). The designs have been obtained for the following objective vectors: (a) $f_0 = 4.2$ GHz, $\varepsilon_r = 2.5$, (b) $f_0 = 3.8$ GHz, $\varepsilon_r = 4.1$, (c) $f_0 = 3.0$ GHz, $\varepsilon_r = 4.4$. The target operating band marked using the vertical lines. Reflection and realized gain characteristics shown using black and gray lines, respectively.

reference designs corresponding to $\{f_0, \varepsilon_r\} = \{2.5, 4.5\}$, $\{3.5, 4.5\}$, $\{5.0, 4.5\}$, $\{2.5, 2.5\}$, $\{5.0, 2.5\}$, $\{3.5, 2.5\}$, $\{4.5, 3.5\}$, and $\{3.0, 3.5\}$ (f_0 in GHz).

The surrogate model is set up for several numbers of principal directions $K = 3$, 4, and 5 ($T = 0.25$ mm). The nested kriging model used as one of the benchmark techniques was constructed using $T = 0.05$. The results are gathered in Table 7, see also Fig. 30. The conventional surrogates demonstrate poor quality (error higher than 30 percent even for 800 training samples). The nested kriging model is more reliable with the practically useful predictive power

TABLE 7. Nested kriging with domain dimensionality reduction: Modeling results for Quasi-Yagi antenna of Fig. 29.

Number of training samples	Relative RMS Error					
	Conventional Models		Nested Kriging Model [70]	Nested Kriging with PCA [94]		
	Kriging	RBF		$K = 3$	$K = 4$	$K = 5$
50	61.4 %	65.3 %	17.9 %	7.9 %	8.5 %	11.7 %
100	50.7 %	51.8 %	13.3 %	6.6 %	7.1 %	6.2 %
200	39.8 %	43.2 %	7.5 %	5.1 %	5.5 %	5.5 %
400	32.8 %	37.1 %	5.4 %	3.8 %	4.5 %	4.5 %
800	31.8 %	33.6 %	4.5 %	3.5 %	4.1 %	4.4 %

achieved for at least 200 training samples. The surrogate with dimensionality reduction is significantly better: the usable accuracy is already obtained for 100 samples.

It should be noted that the first two principal components are dominant for this antenna (normalized eigenvalues equal to $\lambda_1 = 1.00$ and $\lambda_2 = 0.23$), whereas the remaining λ-s are significantly smaller ($\lambda_3 = 0.05$, $\lambda_4 = 0.04$, $\lambda_5 = 0.008$). This indicates that using four principal directions is sufficient. Application case studies shown in Fig. 31 confirm this conclusion: the designs obtained by optimizing the surrogate model described in this section are comparable to those rendered with the use of the nested kriging model.

IV. CONCLUSION

This article summarized the recent developments of the nested kriging framework, a procedure for constructing reliable surrogate models of high-frequency components and structures. Nested kriging belongs to the class of performance-driven modeling methods that rely on appropriate confinement of the model domain. The aim is to focus the modeling process on the relevant parts of the parameter space, specifically those that contain high-quality designs with respect to the considered performance figures. The computational benefits include considerable reduction of the number of training data samples required to set up a reliable surrogate but also a possibility of rendering models over broad ranges of system parameters and operating conditions, beyond the capabilities of conventional techniques.

In this work, we briefly recalled the basic formulation of nested kriging and discussed its recent developments. These advancements concern all major aspects of the techniques, including the improvements of design of experiments, automation of the setup of the control parameters, as well as the various approaches to improve further the predictive power of the nested kriging surrogate. The latter include variable-thickness domain, incorporation of variable-fidelity simulation models, a combination of the nested kriging framework with response feature technology, and explicit reduction of the model domain dimensionality using the spectral analysis of the reference set. Finally, a technique for reducing the number of reference designs (directly affecting the initial setup cost of the surrogate) using gradient-enhanced kriging has been discussed as well. The presented approaches can be used to extend the range of applicability of nested kriging to higher-dimensional cases but also to lower the computational cost of training data acquisition.

Our discussions have been illustrated using a large number of real-world high-frequency test cases, both antenna and microwave components and enhanced using comprehensive comparative studies. The authors believe that this work may be useful for the readers interested in alternative approaches to surrogate modeling of high-frequency structures and increase the awareness of the potential of performance-driven methods in terms of what they may offer as compared to traditional techniques.

ACKNOWLEDGMENT

The authors would like to thank Dassault Systemes, France, for making CST Microwave Studio available.

REFERENCES

[1] O. A. Iupikov, M. V. Ivashina, N. Skou, C. Cappellin, K. Pontoppidan, and C. G. M. van 't Klooster, "Multibeam focal plane arrays with digital beamforming for high precision space-borne ocean remote sensing," *IEEE Trans. Antennas Propag.*, vol. 66, no. 2, pp. 737–748, Feb. 2018.

[2] K. R. Jha, B. Bukhari, C. Singh, G. Mishra, and S. K. Sharma, "Compact planar multistandard MIMO antenna for IoT applications," *IEEE Trans. Antennas Propag.*, vol. 66, no. 7, pp. 3327–3336, Jul. 2018.

[3] J. M. Felicio, J. M. Bioucas-Dias, J. R. Costa, and C. A. Fernandes, "Antenna design and near-field characterization for medical microwave imaging applications," *IEEE Trans. Antennas Propag.*, vol. 67, no. 7, pp. 4811–4824, Jul. 2019.

[4] M. Ikram, N. Nguyen-Trong, and A. Abbosh, "Hybrid antenna using open-ended slot for integrated 4G/5G mobile application," *IEEE Antennas Wireless Propag. Lett.*, vol. 19, no. 4, pp. 710–714, Apr. 2020.

[5] A. Meredov, K. Klionovski, and A. Shamim, "Screen-printed, flexible, parasitic beam-switching millimeter-wave antenna array for wearable applications," *IEEE Open J. Antennas Propag.*, vol. 1, pp. 2–10, Nov. 2020.

[6] P. Anacleto, H. Dinis, J. Fernandes, and P. M. Mendes, "Design and characterization of 3-D self-folded microantennas for implantable microdevices," *IEEE Trans. Antennas Propag.*, vol. 68, no. 3, pp. 2031–2039, Mar. 2020.

[7] S. Trinh-Van, Y. Yang, K.-Y. Lee, and K. C. Hwang, "Single-fed circularly polarized dielectric resonator antenna with an enhanced axial ratio bandwidth and enhanced gain," *IEEE Access*, vol. 8, pp. 41045–41052, 2020.

[8] Z. Tang, J. Liu, and Y. Yin, "Enhanced cross-polarization discrimination of wideband differentially fed dual-polarized antenna via a shorting loop," *IEEE Antennas Wireless Propag. Lett.*, vol. 17, no. 8, pp. 1454–1458, Aug. 2018.

[9] J. Y. Siddiqui, C. Saha, and Y. M. M. Antar, "A novel ultrawideband (UWB) printed antenna with a dual complementary characteristic," *IEEE Antennas Wireless Propag. Lett.*, vol. 14, pp. 974–977, Dec. 2015.

[10] H. Zou, Y. Li, B. Xu, Y. Chen, H. Jin, G. Yang, and Y. Luo, "Dual-functional MIMO antenna array with high isolation for 5G/WLAN applications in smartphones," *IEEE Access*, vol. 7, pp. 167470–167480, 2019.

[11] Z. Ren, A. Zhao, and S. Wu, "MIMO antenna with compact decoupled antenna pairs for 5G mobile terminals," *IEEE Antennas Wireless Propag. Lett.*, vol. 18, no. 7, pp. 1367–1371, Jul. 2019.

[12] Z. Liang, S. Lv, Y. Li, J. Liu, and Y. Long, "Compact folded slot antenna and its endfire arrays with high gain and vertical polarization," *IEEE Antennas Wireless Propag. Lett.*, vol. 19, no. 5, pp. 786–790, May 2020.

[13] A. Contreras, M. Ribo, L. Pradell, V. Raynal, I. Moreno, M. Combes, and M. Ten, "Compact fully uniplanar bandstop filter based on slow-wave multimodal CPW resonators," *IEEE Microw. Wireless Compon. Lett.*, vol. 28, no. 9, pp. 780–782, Sep. 2018.

[14] C.-H. Tseng and C.-L. Chang, "A rigorous design methodology for compact planar branch-line and rat-race couplers with asymmetrical T-structures," *IEEE Trans. Microw. Theory Techn.*, vol. 60, no. 7, pp. 2085–2092, Jul. 2012.

[15] S. Kim and S. Nam, "A compact and wideband linear array antenna with low mutual coupling," *IEEE Trans. Antennas Propag.*, vol. 67, no. 8, pp. 5695–5699, Aug. 2019.

[16] P. S. M. Yazeen, C. V. Vinisha, S. Vandana, M. Suprava, and R. U. Nair, "Electromagnetic performance analysis of graded dielectric inhomogeneous streamlined airborne radome," *IEEE Trans. Antennas Propag.*, vol. 65, no. 5, pp. 2718–2723, May 2017.

[17] P. Prabhu and S. Malarvizhi, "Novel double-side EBG based mutual coupling reduction for compact quad port UWB MIMO antenna," *AEU-Int. J. Electron. Commun.*, vol. 109, pp. 146–156, Sep. 2019.

[18] E. Hassan, D. Noreland, R. Augustine, E. Wadbro, and M. Berggren, "Topology optimization of planar antennas for wideband near-field coupling," *IEEE Trans. Antennas Propag.*, vol. 63, no. 9, pp. 4208–4213, Sep. 2015.

[19] M. A. Fakih, A. Diallo, P. Le Thuc, R. Staraj, O. Mourad, and E. A. Rachid, "Optimization of efficient dual band PIFA system for MIMO half-duplex 4G/LTE and full-duplex 5G communications," *IEEE Access*, vol. 7, pp. 128881–128895, 2019.

[20] K. Tsukamoto and H. Arai, "Optimization of smooth walled horn antenna using multilevel fast multipole method," in *Proc. IEEE Int. Symp. Antennas Propag. (ISAP)*, Okinawa, Japan, Oct. 2016, pp. 24–28.

[21] J. A. Easum, J. Nagar, P. L. Werner, and D. H. Werner, "Efficient multiobjective antenna optimization with tolerance analysis through the use of surrogate models," *IEEE Trans. Antennas Propag.*, vol. 66, no. 12, pp. 6706–6715, Dec. 2018.

[22] J. Zhang, C. Zhang, F. Feng, W. Zhang, J. Ma, and Q.-J. Zhang, "Polynomial chaos-based approach to yield-driven EM optimization," *IEEE Trans. Microw. Theory Techn.*, vol. 66, no. 7, pp. 3186–3199, Jul. 2018.

[23] J. A. Tomasson, S. Koziel, and A. Pietrenko-Dabrowska, "Expedited design closure of antenna input characteristics by trust region gradient search and principal component analysis," *IEEE Access*, vol. 8, pp. 8502–8511, 2020.

[24] S. Koziel and A. Pietrenko-Dabrowska, "Rapid multi-objective optimization of antennas using nested Kriging surrogates and single-fidelity EM simulation models," *Eng. Comput.*, vol. 37, no. 4, pp. 1491–1512, Dec. 2019.

[25] A. Kaintura, T. Dhaene, and D. Spina, "Review of polynomial chaos-based methods for uncertainty quantification in modern integrated circuits," *Electronics*, vol. 7, no. 3, p. 30, Feb. 2018.

[26] A. Pietrenko-Dabrowska, "Rapid tolerance-aware design of miniaturized microwave passives by means of confined-domain surrogates," *Int. J. Numer. Model., Electron. Netw., Devices Fields*, vol. 33, no. 6, Jul. 2020, Art. no. e2779.

[27] A. Lalbakhsh, M. U. Afzal, and K. P. Esselle, "Multiobjective particle swarm optimization to design a time-delay equalizer metasurface for an electromagnetic band-gap resonator antenna," *IEEE Antennas Wireless Propag. Lett.*, vol. 16, pp. 912–915, 2017.

[28] L. Seyyed Kalantari, O. S. Ahmed, M. H. Bakr, and N. K. Nikolova, "A TLM-based wideband adjoint variable method for sensitivity analysis of non-dispersive anisotropic structures," *IEEE Trans. Antennas Propag.*, vol. 65, no. 10, pp. 5267–5278, Oct. 2017.

[29] S. Koziel and A. Pietrenko-Dabrowska, "Reduced-cost electromagnetic-driven optimisation of antenna structures by means of trust-region gradient-search with sparse jacobian updates," *IET Microw., Antennas Propag.*, vol. 13, no. 10, pp. 1646–1652, Aug. 2019.

[30] A. Pietrenko-Dabrowska and S. Koziel, "Computationally-efficient design optimisation of antennas by accelerated gradient search with sensitivity and design change monitoring," *IET Microw., Antennas Propag.*, vol. 14, no. 2, pp. 165–170, Feb. 2020.

[31] S. Koziel and A. Pietrenko-Dabrowska, "Expedited optimization of antenna input characteristics with adaptive Broyden updates," *Eng. Comput.*, vol. 37, no. 3, pp. 851–862, 2020.

[32] J. E. Rayas-Sanchez, "Power in simplicity with ASM: Tracing the aggressive space mapping algorithm over two decades of development and engineering applications," *IEEE Microw. Mag.*, vol. 17, no. 4, pp. 64–76, Apr. 2016.

[33] J. C. Cervantes-González, J. E. Rayas-Sánchez, C. A. López, J. R. Camacho-Pérez, Z. Brito-Brito, and J. L. Chávez-Hurtado, "Space mapping optimization of handset antennas considering EM effects of mobile phone components and human body," *Int. J. RF Microw. Comput.-Aided Eng.*, vol. 26, no. 2, pp. 121–128, Feb. 2016.

[34] S. Koziel and S. D. Unnsteinsson, "Expedited design closure of antennas by means of Trust-Region-Based adaptive response scaling," *IEEE Antennas Wireless Propag. Lett.*, vol. 17, no. 6, pp. 1099–1103, Jun. 2018.

[35] S. Koziel, Q. S. Cheng, J. W. Bandler, and S. Ogurtsov, "Rapid electromagnetic-based microwave design optimisation exploiting shape-preserving response prediction and adjoint sensitivities," *IET Microw., Antennas Propag.*, vol. 8, no. 10, pp. 775–781, Jul. 2014.

[36] S. Koziel, "Fast simulation-driven antenna design using response-feature surrogates," *Int. J. RF Microw. Comput.-Aided Eng.*, vol. 25, no. 5, pp. 394–402, Jun. 2015.

[37] S. Koziel and A. Pietrenko-Dabrowska, "Expedited feature-based quasi-global optimization of multi-band antenna input characteristics with jacobian variability tracking," *IEEE Access*, vol. 8, pp. 83907–83915, 2020.

[38] C. Zhang, F. Feng, Q.-J. Zhang, and J. W. Bandler, "Enhanced cognition-driven formulation of space mapping for equal-ripple optimisation of microwave filters," *IET Microw., Antennas Propag.*, vol. 12, no. 1, pp. 82–91, Sep. 2017.

[39] A. M. Alzahed, S. M. Mikki, and Y. M. M. Antar, "Nonlinear mutual coupling compensation operator design using a novel electromagnetic machine learning paradigm," *IEEE Antennas Wireless Propag. Lett.*, vol. 18, no. 5, pp. 861–865, May 2019.

[40] D. R. Prado, J. A. Lopez-Fernandez, M. Arrebola, and G. Goussetis, "Support vector regression to accelerate design and crosspolar optimization of shaped-beam reflectarray antennas for space applications," *IEEE Trans. Antennas Propag.*, vol. 67, no. 3, pp. 1659–1668, Mar. 2019.

[41] T. Mandic, M. Magerl, and A. Baric, "Sequential buildup of broadband equivalent circuit model for low-cost SMA connectors," *IEEE Trans. Electromagn. Compat.*, vol. 61, no. 1, pp. 242–250, Feb. 2019.

[42] C. Zhang, F. Feng, V.-M.-R. Gongal-Reddy, Q. J. Zhang, and J. W. Bandler, "Cognition-driven formulation of space mapping for equal-ripple optimization of microwave filters," *IEEE Trans. Microw. Theory Techn.*, vol. 63, no. 7, pp. 2154–2165, Jul. 2015.

[43] F. Feng, J. Zhang, W. Zhang, Z. Zhao, J. Jin, and Q.-J. Zhang, "Coarse- and fine-mesh space mapping for EM optimization incorporating mesh deformation," *IEEE Microw. Wireless Compon. Lett.*, vol. 29, no. 8, pp. 510–512, Aug. 2019.

[44] X. Wang, G. G. Wang, B. Song, P. Wang, and Y. Wang, "A novel evolutionary sampling assisted optimization method for high-dimensional expensive problems," *IEEE Trans. Evol. Comput.*, vol. 23, no. 5, pp. 815–827, Oct. 2019.

[45] H. M. Torun and M. Swaminathan, "High-dimensional global optimization method for high-frequency electronic design," *IEEE Trans. Microw. Theory Techn.*, vol. 67, no. 6, pp. 2128–2142, Jun. 2019.

[46] S. N. Lophaven, H. B. Nielsen, and J. ans Søndergaard, "DACE: A MATLAB Kriging toolbox," Tech. Univ. Denmark, Lyngby, Denmark, Tech. Rep. DK-2800, 2002.

[47] D. Gorissen, K. Crombecq, I. Couckuyt, T. Dhaene, and P. Demeester, "A surrogate modeling and adaptive sampling toolbox for computer based design," *J. Mach. Learn. Res.*, vol. 11, pp. 2051–2055, Jul. 2010.

[48] N. V. Queipo, R. T. Haftka, W. Shyy, T. Goel, R. Vaidyanathan, and P. K. Tucker, "Surrogate-based analysis and optimization," *Prog. Aerosp. Sci.*, vol. 41, no. 1, pp. 1–28, 2005.

[49] P. Barmuta, F. Ferranti, G. P. Gibiino, A. Lewandowski, and D. M. M.-P. Schreurs, "Compact behavioral models of nonlinear active devices using response surface methodology," *IEEE Trans. Microw. Theory Techn.*, vol. 63, no. 1, pp. 56–64, Jan. 2015.

[50] J. A. Easum, J. Nagar, and D. H. Werner, "Multi-objective surrogate-assisted optimization applied to patch antenna design," in *Proc. IEEE Int. Symp. Antennas Propag. USNC/URSI Nat. Radio Sci. Meeting*, San Diego, CA, USA, Jul. 2017, pp. 339–340.

[51] D. R. Prado, J. A. Lopez-Fernandez, M. Arrebola, M. R. Pino, and G. Goussetis, "Wideband shaped-beam reflectarray design using support vector regression analysis," *IEEE Antennas Wireless Propag. Lett.*, vol. 18, no. 11, pp. 2287–2291, Nov. 2019.

[52] A. Rawat, R. N. Yadav, and S. C. Shrivastava, "Neural network applications in smart antenna arrays: A review," *AEU-Int. J. Electron. Commun.*, vol. 66, no. 11, pp. 903–912, Nov. 2012.

[53] A. Petrocchi, A. Kaintura, G. Avolio, D. Spina, T. Dhaene, A. Raffo, and D. M. M.-P. Schreurs, "Measurement uncertainty propagation in transistor model parameters via polynomial chaos expansion," *IEEE Microw. Wireless Compon. Lett.*, vol. 27, no. 6, pp. 572–574, Jun. 2017.

[54] S. Koziel and A. Pietrenko-Dabrowska, *Performance-Driven Surrogate Modeling of High-Frequency Structures*. New York, NY, USA: Springer, 2020.

[55] A.-K.-S. O. Hassan, A. S. Etman, and E. A. Soliman, "Optimization of a novel nano antenna with two radiation modes using Kriging surrogate models," *IEEE Photon. J.*, vol. 10, no. 4, pp. 1–17, Aug. 2018.

[56] A. Kumar, A. Lala, V. K. Singh, and A. K. Bhoi, "Estimation of frequency band of microstrip antenna (MSA) with radial basis function (RBF)," in *Advances in Communication, Devices and Networking* (Lecture Notes in Electrical Engineering), vol. 462, R. Bera, S. Sarkar, and S. Chakraborty, Eds. Singapore: Springer, 2018.

[57] S. Koziel, Q. S. Cheng, J. W. Bandler, and S. Ogurtsov, "Rapid electromagnetic-based microwave design optimisation exploiting shape-preserving response prediction and adjoint sensitivities," *IET Microw., Antennas Propag.*, vol. 8, no. 10, pp. 775–781, Jul. 2014.
[58] A. C. Yucel, H. Bagci, and E. Michielssen, "An ME-PC enhanced HDMR method for efficient statistical analysis of multiconductor transmission line networks," *IEEE Trans. Compon., Packag., Manuf., Technol.*, vol. 5, no. 5, pp. 685–696, May 2015.
[59] M. Xu, M. Chen, and J. Lafferty, "Faithful variable screening for high-dimensional convex regression," *Ann. Statist.*, vol. 44, no. 6, pp. 2624–2660, Dec. 2016.
[60] S. Ding and L. Pichon, "Sensitivity analysis of an implanted antenna within surrounding biological environment," *Energies*, vol. 13, no. 4, p. 996, Feb. 2020.
[61] J. A. Tomasson, A. Pietrenko-Dabrowska, and S. Koziel, "Expedited globalized antenna optimization by principal components and variable-fidelity EM simulations: Application to microstrip antenna design," *Electronics*, vol. 9, no. 4, p. 673, Apr. 2020.
[62] J. A. Tropp, "Greed is good: Algorithmic results for sparse approximation," *IEEE Trans. Inf. Theory*, vol. 50, no. 10, pp. 2231–2242, Oct. 2004.
[63] R. Hu, V. Monebhurrun, R. Himeno, H. Yokota, and F. Costen, "An adaptive least angle regression method for uncertainty quantification in FDTD computation," *IEEE Trans. Antennas Propag.*, vol. 66, no. 12, pp. 7188–7197, Dec. 2018.
[64] M. Kennedy, "Predicting the output from a complex computer code when fast approximations are available," *Biometrika*, vol. 87, no. 1, pp. 1–13, Mar. 2000.
[65] F. Wang, P. Cachecho, W. Zhang, S. Sun, X. Li, R. Kanj, and C. Gu, "Bayesian model fusion: Large-scale performance modeling of analog and mixed-signal circuits by reusing early-stage data," *IEEE Trans. Comput.-Aided Design Integr. Circuits Syst.*, vol. 35, no. 8, pp. 1255–1268, Aug. 2016.
[66] J. P. Jacobs and S. Koziel, "Two-stage framework for efficient Gaussian process modeling of antenna input characteristics," *IEEE Trans. Antennas Propag.*, vol. 62, no. 2, pp. 706–713, Feb. 2014.
[67] S. Koziel, "Low-cost data-driven surrogate modeling of antenna structures by constrained sampling," *IEEE Antennas Wireless Propag. Lett.*, vol. 16, pp. 461–464, 2017.
[68] S. Koziel and A. Bekasiewicz, "On reduced-cost design-oriented constrained surrogate modeling of antenna structures," *IEEE Antennas Wireless Propag. Lett.*, vol. 16, pp. 1618–1621, 2017.
[69] S. Koziel and A. T. Sigurdsson, "Triangulation-based constrained surrogate modeling of antennas," *IEEE Trans. Antennas Propag.*, vol. 66, no. 8, pp. 4170–4179, Aug. 2018.
[70] S. Koziel and A. Pietrenko-Dabrowska, "Performance-based nested surrogate modeling of antenna input characteristics," *IEEE Trans. Antennas Propag.*, vol. 67, no. 5, pp. 2904–2912, May 2019.
[71] S. Koziel and A. Pietrenko-Dabrowska, "Reduced-cost surrogate modelling of compact microwave components by two-level Kriging interpolation," *Eng. Optim.*, vol. 52, no. 6, pp. 960–972, Jun. 2020.
[72] S. Koziel and A. Pietrenko-Dabrowska, "Reliable data-driven modeling of high-frequency structures by means of nested Kriging with enhanced design of experiments," *Eng. Comput.*, vol. 36, no. 7, pp. 2293–2308, Aug. 2019.
[73] A. Pietrenko-Dabrowska and S. Koziel, "Cost-efficient surrogate modeling of high-frequency structures using nested Kriging with automated adjustment of model domain lateral dimensions," *AEU-Int. J. Electron. Commun.*, vol. 121, Jul. 2020, Art. no. 153224.
[74] A. Pietrenko-Dabrowska, S. Koziel, and M. Al-Hasan, "Cost-efficient bi-layer modeling of antenna input characteristics using gradient Kriging surrogates," *IEEE Access*, vol. 8, pp. 140831–140839, 2020.
[75] S. Koziel and A. Pietrenko-Dabrowska, "Low-cost performance-driven modelling of compact microwave components with two-layer surrogates and gradient Kriging," *AEU-Int. J. Electron. Commun.*, vol. 126, Nov. 2020, Art. no. 153419.
[76] S. Koziel and A. Pietrenko-Dabrowska, "Design-oriented computationally-efficient feature-based surrogate modelling of multi-band antennas with nested Kriging," *AEU-Int. J. Electron. Commun.*, vol. 120, Jun. 2020, Art. no. 153202.
[77] S. Koziel and A. Pietrenko-Dabrowska, "Design-oriented modeling of antenna structures by means of two-level Kriging with explicit dimensionality reduction," *AEU-Int. J. Electron. Commun.*, vol. 127, Dec. 2020, Art. no. 153466.
[78] S. Koziel, A. Pietrenko-Dabrowska, and M. Al-Hasan, "Design-oriented two-stage surrogate modeling of miniaturized microstrip circuits with dimensionality reduction," *IEEE Access*, vol. 8, pp. 121744–121754, 2020.
[79] T. W. Simpson, J. D. Poplinski, P. N. Koch, and J. K. Allen, "Metamodels for computer-based engineering design: Survey and recommendations," *Eng. Comput.*, vol. 17, no. 2, pp. 129–150, Jul. 2001.
[80] B. Beachkofski and R. Grandhi, "Improved distributed hypercube sampling," in *Proc. 43rd AIAA/ASME/ASCE/AHS/ASC Struct., Struct. Dyn., Mater. Conf.*, 2002, Art. no. 1274-2002.
[81] C.-Y.-D. Sim, M.-H. Chang, and B.-Y. Chen, "Microstrip-fed ring slot antenna design with wideband harmonic suppression," *IEEE Trans. Antennas Propag.*, vol. 62, no. 9, pp. 4828–4832, Sep. 2014.
[82] S. Koziel and A. Pietrenko-Dabrowska, "Cost-efficient performance-driven modelling of multi-band antennas by variable-fidelity electromagnetic simulations and customized space mapping," *Int. J. Numer. Model., Electron. Netw., Devices Fields*, vol. 33, no. 6, p. e2778, Jul. 2020.
[83] A. Pietrenko-Dabrowska and S. Koziel, "Antenna modeling using variable-fidelity EM simulations and constrained co-Kriging," *IEEE Access*, vol. 8, pp. 91048–91056, 2020.
[84] Y.-C. Chen, S.-Y. Chen, and P. Hsu, "Dual-band slot dipole antenna fed by a coplanar waveguide," in *Proc. IEEE Antennas Propag. Soc. Int. Symp.*, Guilin, China, Jul. 2006, pp. 3589–3592.
[85] S. Ulaganathan, I. Couckuyt, T. Dhaene, E. Laermans, and J. Degroote, "On the use of gradients in Kriging surrogate models," in *Proc. Winter Simulation Conf.*, Savanah, GA, USA, Dec. 2014, pp. 2692–2701.
[86] S. Koziel, "Fast simulation-driven antenna design using response-feature surrogates," *Int. J. RF Microw. Comput.-Aided Eng.*, vol. 25, no. 5, pp. 394–402, Jun. 2015.
[87] S. Koziel, Q. S. Cheng, and J. W. Bandler, "Feature-based surrogates for low-cost microwave modelling and optimisation," *IET Microw., Antennas Propag.*, vol. 9, no. 15, pp. 1706–1712, Dec. 2015.
[88] A. Pietrenko-Dabrowska and S. Koziel, "Surrogate modeling of impedance matching transformers by means of variable-fidelity electromagnetic simulations and nested cokriging," *Int. J. RF Microw. Comput.-Aided Eng.*, vol. 30, no. 8, Aug. 2020, Art. no. e22268.
[89] M. G. N. Alsath and M. Kanagasabai, "Compact UWB monopole antenna for automotive communications," *IEEE Trans. Antennas Propag.*, vol. 63, no. 9, pp. 4204–4208, Sep. 2015.
[90] I.T. Jolliffe, *Principal Component Analysis*, 2nd ed. New York, NY, USA: Springer, 2002.
[91] D. Bau, III, and L. N. Trefethen, *Numerical Linear Algebra*. Philadelphia, PA, USA: SIAM, 1997.
[92] Z. Hua, G. Haichuan, L. Hongmei, L. Beijia, L. Guanjun, and W. Qun, "A novel high-gain quasi-Yagi antenna with a parabolic reflector," in *Proc. Int. Symp. Ant. Prop. (ISAP)*, Hobart, Tas, Australia, Nov. 2015, pp. 1–3.

SLAWOMIR KOZIEL (Senior Member, IEEE) received the M.Sc. and Ph.D. degrees in electronic engineering from the Gdansk University of Technology, Poland, in 1995 and 2000, respectively, and the M.Sc. degrees in theoretical physics and mathematics and the Ph.D. degree in mathematics from the University of Gdansk, Poland, in 2000, 2002, and 2003, respectively. He is currently a Professor with the Department of Engineering, Reykjavik University, Iceland. His research interests include CAD and modeling of microwave and antenna structures, simulation-driven design, surrogate-based optimization, space mapping, circuit theory, analog signal processing, evolutionary computation, and numerical analysis.

ANNA PIETRENKO-DABROWSKA (Senior Member, IEEE) received the M.Sc. and Ph.D. degrees in electronic engineering from the Gdansk University of Technology, Poland, in 1998 and 2007, respectively. She is currently an Associate Professor with the Gdansk University of Technology. Her research interests include simulation-driven design, design optimization, control theory, modeling of microwave and antenna structures, and numerical analysis.